

Article

The Mechanism of Metal-Containing Formate Dehydrogenases Revisited: The Formation of Bicarbonate as Product Intermediate Provides Evidence for an Oxygen Atom Transfer Mechanism

Hemant Kumar ^{1,†} , Maryam Khosraneh ^{2,†}, Siva S. M. Bandaru ², Carola Schulzke ^{2,*} 
and Silke Leimkühler ^{1,*} 

¹ Institute of Biochemistry and Biology, Department of Molecular Enzymology, University of Potsdam, Karl-Liebknecht Strasse 24 H25, 14476 Potsdam, Germany

² Institute for Biochemistry, University of Greifswald, Felix-Hausdorff-Straße 4, 17489 Greifswald, Germany

* Correspondence: carola.schulzke@uni-greifswald.de (C.S.); sleim@uni-potsdam.de (S.L.)

† These authors contributed equally to this work.

Abstract: Mo/W-containing formate dehydrogenases (FDH) catalyzed the reversible oxidation of formate to carbon dioxide at their molybdenum or tungsten active sites. While in the reaction of formate oxidation, the product is CO₂, which exits the active site via a hydrophobic channel; bicarbonate is formed as the first intermediate during the reaction at the active site. Other than what has been previously reported, bicarbonate is formed after an oxygen atom transfer reaction, transferring the oxygen from water to formate and a subsequent proton-coupled electron transfer or hydride transfer reaction involving the sulfido ligand as acceptor.

Keywords: molybdoenzyme; formate dehydrogenase; oxygen atom transfer; *Rhodobactor capsulatus*



Citation: Kumar, H.; Khosraneh, M.; Bandaru, S.S.M.; Schulzke, C.; Leimkühler, S. The Mechanism of Metal-Containing Formate Dehydrogenases Revisited: The Formation of Bicarbonate as Product Intermediate Provides Evidence for an Oxygen Atom Transfer Mechanism. *Molecules* **2023**, *28*, 1537. <https://doi.org/10.3390/molecules28041537>

Academic Editor: Ralf R. Mendel

Received: 10 December 2022

Revised: 31 January 2023

Accepted: 2 February 2023

Published: 5 February 2023



Copyright: © 2023 by the authors. Licensee MDPI, Basel, Switzerland. This article is an open access article distributed under the terms and conditions of the Creative Commons Attribution (CC BY) license (<https://creativecommons.org/licenses/by/4.0/>).

1. Introduction

The biological reduction of carbon dioxide (CO₂) involves the conversion of a highly stable and chemically inert compound into more reactive and useful organic chemicals, representing a key process in the global carbon cycle that is of high relevance for combating the greenhouse effect [1]. Among these enzymes, formate dehydrogenases (FDHs) represent a diverse group of enzymes in bacteria, archaea, and eukaryotes that have been proposed to facilitate the reversible two electron and one proton abstraction of formate to produce CO₂ by catalyzing the following redox reaction, with the equilibrium being on the side of formate oxidation [2,3]:



Enzymatic reduction in CO₂ to formate would allow for the storage of hydrogen as a fuel for industrial applications [4–6] as well as carbon sequestration from the atmosphere [1,7], rendering these enzymes interesting targets for biotechnological utilization.

In general, most of the FDH enzymes catalyze preferentially the forward reaction of formate oxidation [8]. The released electrons are transferred in intramolecular electron transfer reactions for the eventual reduction of one of several terminal electron acceptors. Some metal-containing enzymes, however, were described to act rather as CO₂ reductases [9], reducing CO₂ to formate [10]. Metal-containing FDHs belong to the family of molybdenum/tungsten cofactor-containing enzymes, binding the bis-Metal-binding pterin Guanine Dinucleotide (bis-MGD) cofactor at their active site [11]. In the bis-MGD cofactor, the metal center is coordinated by two pterin ene-dithiolates, a sulfur atom, and either a cysteine or selenocysteine [12]. FDHs containing the latter ligand were found to be rather

oxygen-sensitive [3,12]. All FDHs contain two additional highly conserved residues in the active site, a histidine and an arginine [13,14]. The reaction of formate/CO₂ interconversion occurs at the molybdenum or tungsten metal ion in the bis-MGD cofactor, in which the metal (M) cycles between the M^{VI}, M^V, and M^{IV} oxidation states during the reaction [15]. Close to the (bis-MGD) cofactor, a proximal [4Fe–4S] cluster is present in all metal-containing FDH enzymes [16], which is involved in the intramolecular electron transfer reaction. In *Rhodobacter capsulatus* FDH, the oxidation of formate is energetically coupled to the reduction in oxidized nicotinamide adenine dinucleotide (NAD⁺) in the cytosol [17].

While metal-dependent FDH enzymes have been studied for several decades and the *E. coli*, the FdhF enzyme was among the first molybdoenzymes to be crystallized [12]. Details of the reaction mechanism remain only poorly understood and the overall catalytic mechanism of formate oxidation is still under debate [2,18].

It was reported [19–21] that the reaction of metal-containing FDHs do not constitute the characteristic oxygen atom transfer reaction, as typically catalyzed by the DMSO reductase family of Mo/W bis-MGD-containing enzymes [22]. Instead, it has been suggested that the reaction involves only the heterolytic fission of the C–H bond facilitated through a direct hydride transfer to the terminal sulfido ligand at the molybdenum atom, with the immediate product being CO₂ and not bicarbonate [19,20]. This hypothesis was first proposed by Thauer et al. (1975) in the characterization of the FDH (ferredoxin: CO₂ oxidoreductase) from *Clostridium pasteurianum* [19]. It was later supported by a study from Khangulov et al. (1998) [21] on *Escherichia coli* FdhF, who investigated product formation using GC-MS with ¹³C-labeled formate in ¹⁸O-enriched water, which resulted in the detection of only ¹³CO₂ gas without any ¹⁸O atoms.

A recent study by Meneghello et al. (2021) [20] applied an electrochemical approach to the tungsten-containing FDH from *Desulfovibrio vulgaris* Hildenborough [23] to confirm conclusions from earlier cumulative work; i.e., that the substrate of FDHs for the back reaction of CO₂ reduction is CO₂ rather than HCO₃[−]. However, as already pointed out by Cooper et al. (1968) [24], it still remains possible that these observations are more a reflection of the binding of the preferred molecule to the active site and do not necessarily reflect what is happening during substrate turnover, especially since the product formation was not quantified in the assay, and by electrochemistry it cannot be determined which substrate is bound at the active site and which ligands are involved in the binding. It, therefore, might be possible that charged HCO₃[−] is hindered from entering the active site via the hydrophobic channel that has been identified in crystal and cryo-EM structures of FDH enzymes, while CO₂ in contrast can easily enter [23,25]. At the active site, CO₂ could react with H₂O to form HCO₃[−] which then acts as the actual substrate for the reaction, which is only formally the reduction of CO₂ [19]. This option has, so far, been unconsidered in most respective studies [2,10,13,15,18,21,23]. It should, however, attract more attention, since in some X-ray structures of FDH enzymes a water molecule was identified in the active site which is bound in the vicinity to the conserved arginine residue in the second coordination sphere [23,26,27]. It is not unlikely that H₂¹⁸O progression into the active site of the enzyme and its exchange with unlabeled water therein is slow, if the enzyme and active site are saturated with unlabeled water. This might be one of the reasons why Khangulov et al. did not detect an ¹⁸O-labeled CO₂ product in their approach [21].

Here, we reinvestigated the oxygen atom transfer from H₂O¹⁸ to formate yielding C¹⁸O¹⁶O and present the identification of bicarbonate as the first intermediate in the reaction of formate oxidation, before CO₂ is produced in the secondary reaction. We provide clear evidence that metal-containing FDHs catalyze a typical oxygen atom transfer (OAT) reaction. This work revises the 25-year-old hypothesis that FDHs represent an exception in the family of Mo/W-containing enzymes by catalyzing a heterolytic C–H bond cleavage reaction instead of OAT [21]. We also show for the back reaction, that CO₂ and not bicarbonate enters the active site, likely by the proposed hydrophobic channel, but at the active site, first bicarbonate is formed likely in a carbonic anhydrase-like reaction before

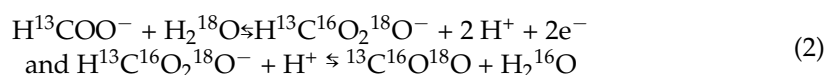
formate is released, as evidenced by using the enzyme soaked in H_2^{18}O labeled water and a $^{13}\text{CO}_2$ saturated buffer, which resulted in the production of $\text{H}^{13}\text{C}^{16}\text{O}^{18}\text{O}^-$ labeled formate.

2. Results

2.1. ^{13}C -Labeled Formate Oxidation by R_cFDH in the Presence of ^{18}O -Labeled Water

We reanalyzed the experiment performed in 1998 by Khangulov et al. [21] with a few modifications using purified *R. capsulatus* FDH, ^{13}C -labeled formate, and ^{18}O -enriched water to determine the amount of ^{18}O in the immediate $^{13}\text{CO}_2$ reaction product. The usage of *R. capsulatus* FDH is advantageous compared to *E. coli* FDH since the enzyme is more oxygen stable, whereby the experiment can be performed in the absence of high inhibitor concentrations of, e.g., azide [28]. Azide might interfere with the reaction as it is a mixed-type inhibitor to formate and interacts with both the CO_2 and the formate-binding moieties in the active site [29,30]. Further, the reaction of formate oxidation of *R. capsulatus* FDH is 77 times slower as compared to *E. coli* FdhF, which facilitates detecting the reaction product [17,31]. However, *R. capsulatus* FDH has a pH optimum of 9.0, which is expected to increase the equilibrium constant of the secondary $^{13}\text{CO}_2 + \text{H}_2^{18}\text{O} \rightleftharpoons \text{H}_2^{13}\text{COO}^{18}\text{O} \rightleftharpoons \text{H}^{13}\text{COO}^{18}\text{O}^- + \text{H}^+$ reaction [17]. To avoid interferences with the secondary reaction at higher pH, we performed the reaction at 10 °C and 25 °C in comparison (Figure 1a,b) since at temperatures below 20 °C and in the absence of carbonic anhydrase, the non-enzymatic hydration of CO_2 is slow [24].

Mass spectrometric analysis of the isotopic composition of CO_2 gas, released upon enzymatic oxidation of ^{13}C -labeled formate ($^{13}\text{COO}^-$) in ^{18}O enriched water (H_2^{18}O), was performed to study the formation of ^{18}O enriched CO_2 ($^{13}\text{C}^{16}\text{O}^{18}\text{O}$) [21]. When H_2^{18}O is used as the oxygen atom source, $\text{H}^{13}\text{C}^{16}\text{O}_2^{18}\text{O}^-$ bicarbonate is the direct formate oxidation product from which $^{13}\text{C}^{16}\text{O}^{18}\text{O}$ is produced (as a major product along with minor amounts of C^{16}O_2) in the secondary reaction by the dehydration of bicarbonate according to the following overall reaction sequence:



^{13}C -labeled formate oxidation by R_cFDH in the presence of 10% ^{18}O labeled water was carried out at pH 9 and the ratio of the product isotope content for $^{13}\text{C}^{16}\text{O}^{18}\text{O}/^{13}\text{C}^{16}\text{O}^{16}\text{O}$ was determined after 10 s, 40 s, 1 min, and 4 min (Figure 1a) at 10 °C and 25 °C (Figure 1a,b).

In the uncatalyzed reaction, $\text{NaH}^{13}\text{CO}_3$ was also converted to $^{13}\text{C}^{16}\text{O}^{18}\text{O}$ in the chemical equilibration of bicarbonate, carbonic acid, and CO_2 but substantially more slowly. We obtained a ratio of 0.005 after 10 s for the uncatalyzed reaction and a ratio of 0.012 for the catalyzed reaction at 10 °C (Figure 1a). At 25 °C, the ratio for the uncatalyzed reaction increased to 0.006 after 10 s and to 0.03 after 4 min (Figure 1b).

The catalyzed reaction, however, produces higher relative amounts of $^{13}\text{C}^{16}\text{O}^{18}\text{O}$ compared to the uncatalyzed reaction under any investigated circumstances, and these ratios are significantly higher in the cold throughout, as well as after 4 min at 25 °C. This supports oxygen from water being primarily inserted into CO_2 enzymatically and not only by an uncatalyzed secondary hydration of $^{13}\text{CO}_2$ with H_2^{18}O from the solvent. After 10 s, the ratio of 0.012 in the catalyzed reaction is lower than the theoretically expected value of 0.066, which most likely goes back to a slow $\text{H}_2\text{O}/\text{H}_2^{18}\text{O}$ exchange rate in the enzyme active site. After 40 s, 1 min, and 4 min, the ratio increased to 0.016 in the enzymatic reaction (Figure 1a). When the percentage of labeled H_2^{18}O content was raised from 10 to 25%, a two-times higher ratio $^{13}\text{C}^{16}\text{O}^{18}\text{O}/^{13}\text{C}^{16}\text{O}^{16}\text{O}$ was observed after 40 s at 10 °C (Figure 1c), demonstrating that H_2^{18}O exchange in the enzyme is a limiting factor at this temperature. The higher ratios of the catalyzed reaction differentiate it from the background reaction and show that FDH catalyzed the oxygen atom transfer from H_2^{18}O to ^{13}C -labeled formate yielding $^{13}\text{C}^{16}\text{O}^{18}\text{O}$.

In contrast to the report by Khangulov et al. [21], we determine an immediate insertion of ^{18}O from H_2^{18}O water into CO_2 already 10 s after the start of the reaction, underlining that an oxygen atom transfer reaction for this enzyme has to be considered. The different observations then and now might be based on the absence of the inhibitor azide in our study, while in the previous investigation of the *E. coli* enzyme, 3 mM azide was present to slow down the reaction. When the reaction was performed with only 1 mM azide added and the *R. capsulatus* enzyme, indeed, almost no ^{18}O labeled $^{13}\text{CO}_2$ was detected within the first 10 s of the reaction (Figure 1d).

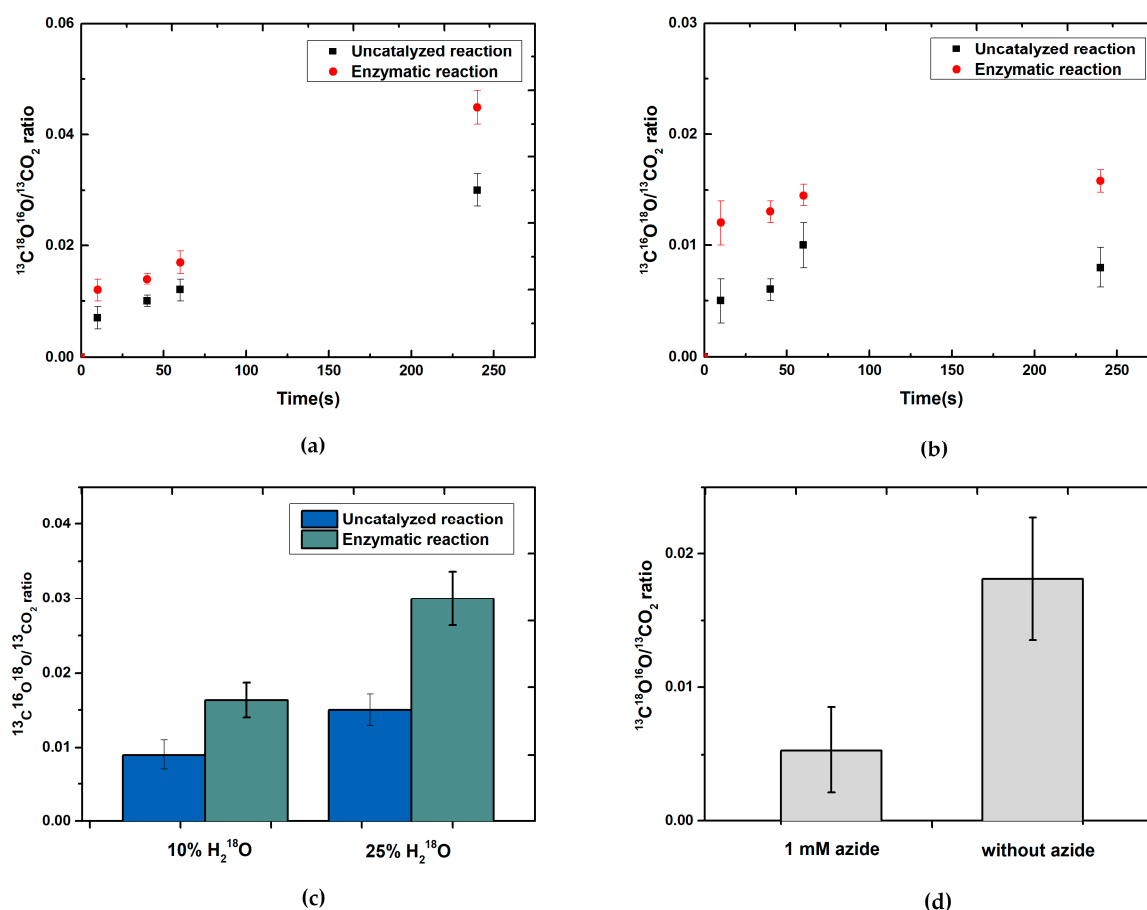


Figure 1. Time-dependent ratios of CO_2 isotopomer ($^{13}\text{C}^{18}\text{O}_2/^{13}\text{CO}_2$) formation at 10 °C (a) and 25 °C (b) using *R. capsulatus* FDH (pH 9) to monitor the enzymatic oxidation of ^{13}C -labeled formate in the presence of 10% H_2^{18}O . The reaction was started by the addition of 30 μM of FDH preincubated with H_2^{18}O to MS vials which contained 10 mM $\text{H}^{13}\text{COO}^-$ 5mM NAD^+ in 100 mM Tris-HCl, pH 9. To avoid any changes in equilibrium, samples were taken directly at the indicated timepoints. Headspace samples were analyzed by GC-MS. The uncatalyzed reaction contained the same components without the enzyme. Additionally, up to 100 mM of $\text{NaH}^{13}\text{CO}_3$ was used in uncatalyzed reactions as a $^{13}\text{CO}_2$ source to monitor the secondary reaction of non-enzymatic CO_2 hydration. (c) Ratios of CO_2 isotopomer ($^{13}\text{C}^{18}\text{O}_2/^{13}\text{CO}_2$) formation after 40 s using different amounts of H_2^{18}O for ^{13}C -labeled formate oxidation using *R. capsulatus* FDH at pH 9 (25 °C). (d) ^{13}C labeled formate oxidation using *RcFDH* in the presence of 1 mM sodium azide and 10% H_2^{18}O . The reaction was started by the addition of 5 μM FDH preincubated with H_2^{18}O to an MS vial which contained 10 mM $\text{H}^{13}\text{COO}^-$, 5 mM NAD^+ in 100 mM Tris-HCl, pH 9. The headspace sample was taken after 10 s and analyzed by GC-MS. The sample with azide contained an additional 1 mM of sodium azide.

2.2. Solvent Deuterium Kinetic Isotope Effect on the Formate Oxidation Reaction

The results above indicate that FDH catalyzes an oxygen atom transfer reaction, in which water (or hydroxide) might displace the formal hydride leaving the group in formate,

a mechanism that has been observed also in enzymes like phosphite dehydrogenase [29]. Consequently, we also determined the solvent kinetic isotope effect (KIE) using D₂O and H₂¹⁸O water in the reaction. Previous kinetic isotope effect studies using deuterium-labeled formate demonstrated significant isotope effects on V_{max} and V_{max}/K_m^{formate} at lower formate concentrations, indicating that cleaving the C–H bond is at least partially rate-determining for the enzymatic reaction [15,30]. Solvent kinetic isotope studies with D₂O or H₂¹⁸O have not been performed before on FDH enzymes. D₂O has only been used in EPR studies on FDH enzymes from *Cuprividus necator* and *Desulfovibrio desulfuricans* [15,32] showing that in the sample prepared in D₂O, the proton coupling to the Mo^V signal disappeared based on the much weaker nuclear magnetic moment of ²H relative to ¹H, which demonstrates the solvent exchangeability of the coupled proton. The solvent-exchangeable proton was conclusively interpreted to be bound to the sulfido ligand of the molybdenum center, while the non-solvent exchangeable proton was interpreted to be bound to the Cα atom of the amino acid ligand (Cys in case of R_cFDH).

We determined the pH-dependent solvent kinetic isotope effect (KIE) on the rapid reaction kinetics using D₂O and H₂¹⁸O. The primary D₂O KIE ratios for the reaction, as listed in Table 1, exhibit a decrease at higher pH values (Figure 2a). This implies that the deprotonation of water is one of the rate-limiting steps and the KIE is less pronounced at higher pH, when water is more easily deprotonated (pK_a 14). The pre-steady state KIE with D₂O, which was also used in combination with DCOO[−] formate, shows significant isotope effects on V_{max} at lower D₂O concentrations (Figure 2b), an effect which was not/not substantially increased when HCOO[−] was used as the substrate (Table 2). This confirms that water, and hence the oxygen atom transfer reaction, has an effect on the reaction rate in addition to the C–H bond cleavage (or C–D bond cleavage in DCOO[−]).

Table 1. Ratios of initial rate constants using unlabeled water versus 50% deuterium oxide (D₂O) or 50% ¹⁸O labeled water (H₂¹⁸O) demonstrating a kinetic isotope effect for H₂O/D₂O.

| pH | k _{H2O} /k _{D2O} | k _{H2O} /k _{H218O} |
|----------------------|------------------------------------|--------------------------------------|
| 6.5 | 0.92 ± 0.03 | 0.97 ± 0.026 |
| 7 | 1.21 ± 0.048 | 1.18 ± 0.037 |
| 7.5 | 1.03 ± 0.033 | 1.02 ± 0.036 |
| 8 (phosphate buffer) | 1.69 ± 0.068 | 1.21 ± 0.059 |
| 8 (tris-HCl buffer) | 1.45 ± 0.05 | 1.22 ± 0.054 |
| 8.5 | 1.70 ± 0.062 | 1.23 ± 0.06 |
| 9 | 1.51 ± 0.048 | 1.08 ± 0.039 |
| 9.5 | 1.23 ± 0.053 | 1.10 ± 0.049 |

Table 2. The effect of deuterated solvent and the substrate on the reductive half-reaction of FDH. Rapid reaction kinetic measurements were carried out using a stopped-flow spectrophotometer. A total of 2.5 μM of R_cFDH under anaerobic conditions with either D₂O or H₂O containing 50 mM phosphate buffer pH/pD 7.9 was used. Formate and deuterated formate (2.5 mM each) were used. Rapid reaction kinetics were obtained by following changes at 445 nm for 2.2 s. k₁ and k₂ are the first and second kinetic constants obtained for the reductive half-reaction after a triphasic fit. The slowest third phase was not included as it is independent of formate concentration [15].

| | | D ₂ O | | H ₂ O | | H ₂ O | |
|------------------|----------------------------|-----------------------------------|-----------------------------------|------------------|----------------------------|-----------------------------------|-----------------------------------|
| | | k ₁ (s ^{−1}) | k ₂ (s ^{−1}) | | | k ₁ (s ^{−1}) | k ₂ (s ^{−1}) |
| D ₂ O | DCOO [−] (2.5 mM) | 65.77 ± 1.91 | 19.44 ± 2.35 | H ₂ O | DCOO [−] (2.5 mM) | 247.32 ± 18.4 | 39.44 ± 1.81 |
| | HCOO [−] (2.5 mM) | 91.57 ± 2.41 | 15.51 ± 1.13 | | HCOO [−] (2.5 mM) | 263.7 ± 13.88 | 47.5 ± 2.31 |

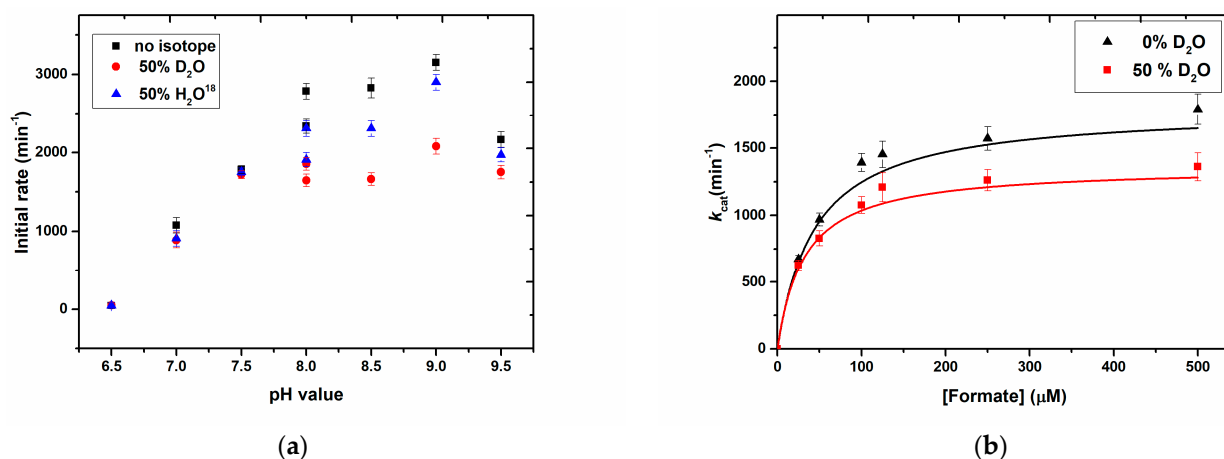


Figure 2. (a) Kinetic solvent isotope effect at different pH using 50% D_2O and 50% H_2^{18}O . The shown ratios were obtained at different pH values. Phosphate buffer (100 mM) for pH 6.5–8.0 and Tris-HCl buffers (100 mM) for pH 8.0–9.5 were used. (b). Kinetic solvent isotope effect on steady-state kinetics using H_2O with 0% and 50% D_2O . Reaction mixture contained 2 mM NAD^+ and formate (50–500 μM) in phosphate buffer (100 mM, pH 7.9). The measurement at 340 nm was started after adding *RcFDH* (50 nM). pH and pD values were corrected, as per the literature [7,33].

2.3. Steady State Kinetics with Monothioformate

We synthesized a sulfur-containing analog of formate, monothioformate, in which one of the oxygen atoms is replaced by sulfur to obtain more insight into the reaction intermediate.

The kinetic constants of purified *R. capsulatus* FDH were determined following the reduction in NAD^+ as the terminal electron acceptor using synthesized monothioformate and dithioformate as substrates. The K_m values for NAD^+ and monothioformate were calculated to be $111.5 \pm 24 \mu\text{M}$ and $3.3 \pm 0.24 \text{ mM}$, respectively, with a k_{cat} of $3032 \pm 83 \text{ min}^{-1}$ from the secondary plot (Figure 3a and Table 3). Taking into account that only 44% of the purified protein was catalytically active in this experiment, the k_{cat} can be calculated as 6890.9 min^{-1} for a fully functional enzyme. The double reciprocal plots with varying monothioformate and NAD^+ concentrations revealed a ping-pong mechanism for the bisubstrate reaction of the enzyme (Figure 3a). Since we have previously proposed a ternary complex mechanism with formate as a substrate, we reinvestigated formate oxidation and also obtained a ping-pong mechanism with a K_m^{formate} of $0.145 \pm 0.025 \text{ mM}$, a $K_m^{\text{NAD}^+}$ of $159.12 \pm 12 \text{ mM}$ and a k_{cat} for the fully active enzyme of 7500 min^{-1} (Table 3). We must, therefore, revise our previously published conclusions and report here that *R. capsulatus* FDH, such as the FDHs from *C. necator* [15] and *E. coli* FdhF [34], also catalyzes formate oxidation and NAD^+ reduction according to a ping-pong mechanism (Figure 3b). The distinct results obtained before are based on too high enzyme concentrations that were used in the respective assay [17]. Most notably, it is shown here that monothioformate acts as a potent substrate for FDH, with k_{cat} values comparable to formate, but with an observed increase in K_m of a factor of 22 (Table 3).

Table 3. Kinetic parameters for the steady state kinetics of *R. capsulatus* FDH for formate and monothioformate as substrates (see also Figure 3).

| Protein | Substrate | k_{cat} (min^{-1}) | K_m Substrate (mM) | K_m NAD^+ (μM) |
|--------------|-----------------|--|----------------------|--|
| <i>RcFDH</i> | Formate | 3300 ± 133 | 0.145 ± 0.025 | 159.12 ± 12 |
| | Monothioformate | 3032 ± 83 | 3.3 ± 0.24 | 111.5 ± 24 |

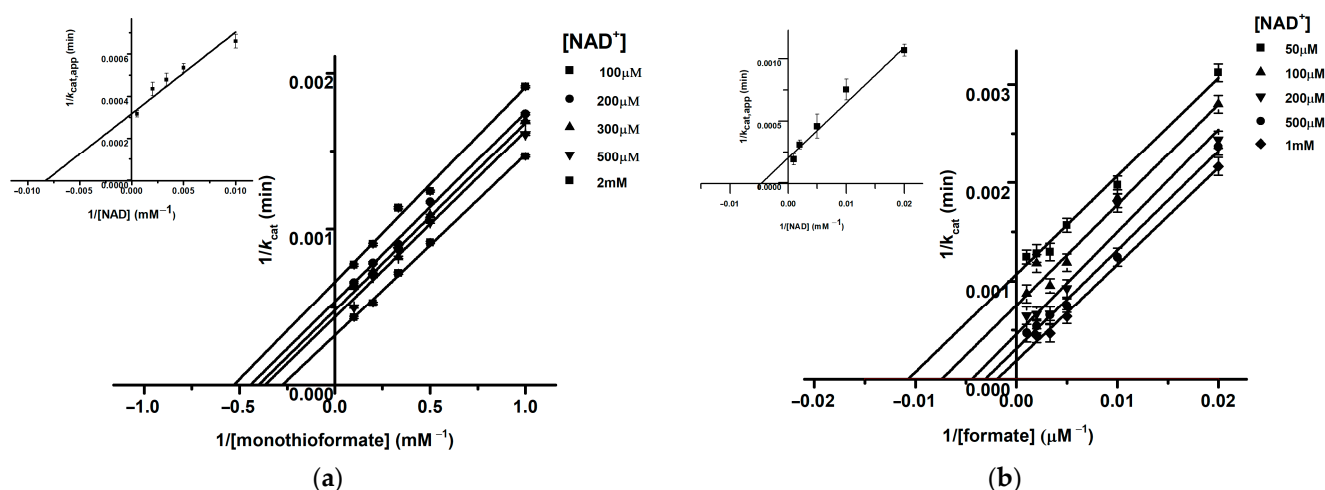


Figure 3. (a) Bisubstrate kinetics of the monothioformate oxidation reaction with NAD^+ as electron acceptor. Lineweaver–Burk plot of k_{cat} using 7 nM FDH with varying thioformate concentrations of 0.5–20 mM and constant NAD^+ concentrations of 100 μM , 200 μM , 300 μM , 500 μM , and 1 mM measured in 100 mM Tris-HCl, pH 9, at room temperature. Inset: the K_i value was obtained from the secondary plot of the apparent $1/V_{\text{max}}$ of the Lineweaver–Burk plot. The data represent the mean values of three independent measurements (\pm standard deviation). (b) Bisubstrate kinetics of the formate oxidation reaction with NAD^+ as electron acceptor. Lineweaver–Burk plot of k_{cat} using 7 nM FDH with varying formate concentrations of 0.5–20 mM and constant NAD^+ concentrations of 500 μM , 100 μM , 200 μM , 500 μM , and 1 mM measured in 100 mM Tris-HCl, pH 9, at room temperature. Inset: the K_m and k_{cat} values were obtained from the secondary plot of the apparent $1/k_{\text{cat,app}}$ intercepts of the Lineweaver–Burk plot. The data represent the mean values of three independent measurements (\pm standard deviation).

In contrast, dithioformate was not accepted as a substrate by *R. capsulatus* FDH and acted instead as a competitive inhibitor (Figure 4), with a K_i of 7.5 mM calculated from the secondary plot.

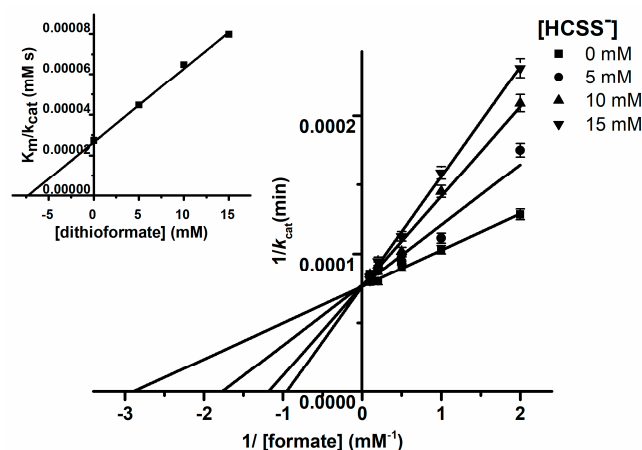


Figure 4. Inhibition kinetics of *RcFDH* with dithioformate. Steady state kinetics were carried out under anaerobic conditions using 2 mM benzyl viologen (ϵ_{578} , benzyl viologen = $8.65 \text{ mM}^{-1}\text{cm}^{-1}$) as an electron acceptor. The assay mixture contained different concentrations of formate (0.05–5 mM), dithioformate (0–15 mM) and 2 mM benzyl viologen in 100 mM Tris-HCl buffer, pH 9. Photometric measurement at 578 nm was carried out for 60 s after the addition of 30 nM *RcFDH*.

2.4. Nuclear Magnetic Resonance Experiments for the Identification of the Reaction Intermediate

Nuclear magnetic resonance (NMR) spectroscopy was chosen to verify the results reported above by a method that not only confirms the elemental composition of the ana-

lytes but also their chemical structure and relative quantity. The observed resonance shifts are directly correlated to the chemical environment of the investigated nucleus. They can be calculated relatively reliably prior to measurement using incremental contributions of binding partners toward the final resonance as a sum of all induced upfield and downfield shifts. However, in the case of this study, all resonances of relevance could be validated based on the literature available. With NMR spectroscopy, it is possible to quantify the relative abundance of the species in solution, which bear NMR-sensitive nuclei. In the case of formate dehydrogenase, the immediate product (bicarbonate/carbonate), as verified by all prior experiments in the course of this investigation and its decomposition product (CO_2), do not bear hydrogen atoms or do not bear those hydrogen atoms, which would be suitable for detection by ^1H -NMR (no rapid exchange allowed). It was, therefore, necessary to turn to less sensitive ^{13}C -NMR spectroscopy, which needs more time per measurement to lead to unambiguous data and a good signal-to-noise ratio (only 1.1% relative abundance of the NMR active nucleus). To counteract this disadvantage and in order to be able to monitor substrate conversion to intermediate (bicarbonate) and the final product (CO_2), it was attempted to slow the enzymatic turnover down by low temperature, pH conditions unfavorable for enzymatic performance, and/or the addition of azide. Still, the enzymatic reactions were too fast to receive unambiguous catalytic data for the transformation by NMR spectroscopy. In order to decrease the duration of the ^{13}C -NMR measurements, ^{13}C -labeled formate was then used as a substrate. The time for each ^{13}C -NMR measurement could, therefore, be reduced to ca. 25 min per run. It was possible to receive a time-dependent series of ^{13}C -NMR spectra with a partial azide-inhibited enzyme at a low temperature (5 °C) and a moderately high pH of 9 monitoring the changes in the NMR resonances of ^{13}C -labeled formate, bicarbonate, and CO_2 . Formate, according to the literature, exhibits a resonance in the ^{13}C -NMR spectrum at 170.5 ppm [35], bicarbonate resonates at 161.3 ppm [36], and CO_2 at 124.0 ppm [37]. The resonances found in this study are in excellent agreement with these published data with 171.37 ppm, 161.28 ppm, and 125.57 ppm, respectively, considering that distinct conditions were applied (see the spectrum in SI, Figure S1). To be entirely certain of the correct assignment and the absence or presence of carbon-bound hydrogen atoms, in addition to the normally proton-decoupled ^{13}C -NMR spectra, proton-coupled spectra were recorded, which confirmed the presence of a C-H moiety for formate and the absence of the same for bicarbonate and CO_2 signals (Figure S2 in the SI).

The results of the time-dependent experiment indicate that the production of bicarbonate precedes the formation of CO_2 , even though a small amount of CO_2 was already present in the first measurement. The substrate was given in large excess and was not consumed by the end of the series. Figure 5A shows the time-dependent development of the maxima of the resonance signals of bicarbonate and CO_2 . CO_2 abundance in the NMR sample tube does only increase significantly after the formation rate of bicarbonate already starts to decrease. Unfortunately, the initial steep rise from zero bicarbonate to the first measurement could not be observed directly, since the enzymatic turnover is still too fast for the time that a single ^{13}C -NMR measurement requires. CO_2 formation, in contrast, accelerates, while bicarbonate formation is already slowing down. This firmly points to bicarbonate as the primarily formed species. The bicarbonate/ CO_2 equilibration in an aqueous solution should start immediately upon the formation of either species in an aqueous solution, even at a pH of 9, and both hypothetical enzymatic mechanisms are generally conceivable: (i) initial formation of CO_2 , which together with water forms carbonic acid, that is then quickly deprotonated at this pH; or (ii) initial formation of bicarbonate, which in aqueous solution becomes partially protonated to carbonic acid and then splits into CO_2 and water. In the former scenario (i) it would be impossible, though, that the ratio of bicarbonate versus CO_2 first rises and then decreases, since the formation of bicarbonate would be entirely dependent on the presence of CO_2 in the first place. Figure 5C shows the development of the bicarbonate: CO_2 ratio over time including measurements after 7 and after 8 days of sample tube storage in the cold, when the concentration of bicarbonate and

CO₂ has apparently reached equilibrium under the applied conditions. This equilibrium has decidedly lower bicarbonate contingent compared to the measurements directly after the enzymatic reaction was started, which is further evidence for the primary formation of bicarbonate and only a secondary, possibly combined enzymatic/non-enzymatic, formation of CO₂ which follows the enzymatic transformation of formate by oxidation and oxygen atom binding to the carbon center.

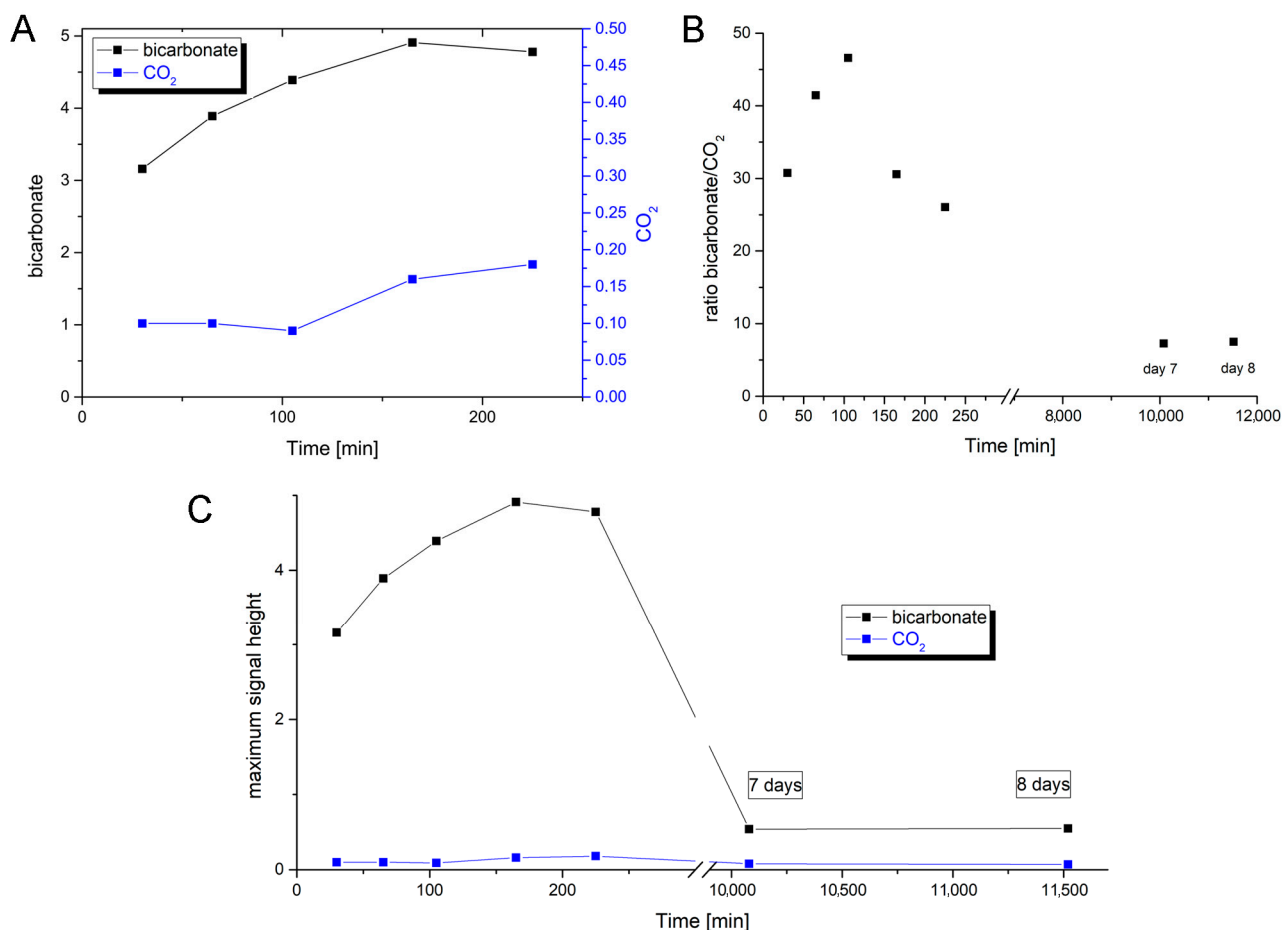


Figure 5. Time-dependent abundance of intermediate and final products of enzymatic formate oxidation. (A) The development of the maxima (signal height) of the resonance signals for bicarbonate (black, left y-axis) and CO₂ (blue, right y-axis) up to 225 min. (B) Time-dependent development of the ratio of bicarbonate content versus CO₂ content derived from the maxima of the resonance signals in the NMR spectra. This includes measurements after 7 and after 8 days to confirm that the bicarbonate/CO₂ equilibrium has settled. (C) The development of maxima (signal height) of the resonance signals for bicarbonate (black) and CO₂ (blue) with a joint y-axis reflecting their relative abundance in the NMR sample tube over time. This includes measurements after 7 and after 8 days to confirm that the bicarbonate/CO₂ equilibrium has settled. The experiment was carried out at 5 °C and pH 9 with an azide-inhibited enzyme and a ¹³C-labeled formate substrate.

In Figure 5C, it can be seen that the overall content of bicarbonate and CO₂ together is decreasing after having reached a maximum at approximately 165 min. The observation further confirms that after the initial production of bicarbonate, this first enzymatic product is transformed into CO₂ which then, likely, leaks into the gas phase of the sample tube. The tube's gas phase does not contribute to the measured signal. From the tube, CO₂ can further leak slowly into the environment since the chosen tube model was not gas-tight for safety reasons. Following the formation of the enzymatic product bicarbonate and its partial transformation to CO₂, the solution, for a short period of time, becomes

oversaturated in CO₂ until eventually the equilibrium is reached with regard to both the reversible conversion between CO₂ and bicarbonate and the solubility of CO₂.

While the obtained data of ¹³C-labeled formate substrate are unambiguous regarding the order of product occurrence, the concomitance of the primary enzymatic reaction and secondary equilibration was still unfavorable for observing continuous product enrichment. In order to vary the reaction kinetics, ¹³C-labeled thioformate was used as a substrate instead of formate, since it was shown in the bisubstrate kinetics that this compound can be used as a substrate by *R. capulatus* FDH with similar k_{cat} values as for formate. These experiments were carried out at room temperature and pH 9 without the addition of an azide inhibitor. The expected signals could be assigned based on the literature values for thioformate (range of 200.5 to 202.9 ppm) [35], thiocarbonate (186.4 ppm) [38], and COS (154.2 ppm) [37]. In this study, the resonances were found in measurements in varied conditions at ca. 211 ppm, 183 ppm, and 159 ppm, respectively; i.e., all slightly shifted from the literature data but unambiguously identified through control and coupling experiments. Notably, (i) the observed resonance for the initial product suggests thiocarbonate rather than thiobicarbonate according to the respective literature and (ii) the final product COS is confirmed to have decidedly better solubility in an aqueous solution than CO₂ since it is polarized (SciFinder provides the value 35 g/L which was calculated for the database/search engine using Advanced Chemistry Development (ACD/Labs) Software V11.02 (© 2023–2021 ACD/Labs)). COS is clearly the dominant species in the thiocarbonate/COS equilibrium even though monothiocarbonic acid is more acidic than carbonic acid (pK_{a1} (H₂CO₂S) = 3.2 [39]; pK_{a1} (H₂CO₃) = 6.35 [40]; N.B.: for carbonic acid, this is the apparent pK_a which is higher than the actual pK_{a1} of 3.88 [41]; the discrepancy goes back to the equilibrium with CO₂). The measurement duration was set in this series to the regular 60 min to obtain spectra of high quality (little noise), sacrificing the glimpse at a more immediate sample composition right after the start of the enzymatic catalysis.

The spectra recorded over time are shown with a range that includes thiocarbonate and COS plus various signals from the NAD⁺/NADH pair (Figure 6A). In the first spectrum which was recorded (and which is essentially a cumulative summary of ca. 1000 recorded scans throughout this first hour), the concentrations of immediate product thiocarbonate and final product COS are almost identical, with thiocarbonate being only marginally more abundant. However, the abundance of thiocarbonate thereafter decreases regularly while the abundance of COS increases regularly and the total abundance first increases slightly (indicating further enzyme activity) and then reaches a plateau (Figure 6B). This proves that the sample has not yet reached enzymatic and solubility equilibrium prior to completion of the first spectrum's recording and, more importantly, that the occurrence of thiocarbonate cannot follow the production of COS but the order must be reversed; i.e., COS can only be formed after the enzyme has produced thiocarbonate (otherwise, the concentration of the latter would not be decreasing). The data firmly support the initial formation of thiocarbonate, followed by transformation to COS, with which it is in an equilibrium that has (in contrast to the formate experiments) a high gas-to-anion ratio; i.e., here, the equilibrium lies on the side of COS. Since this ratio throughout the NMR monitoring constantly increases after the complete consumption of a monothioformate substrate, COS cannot be the initial product of the enzymatic transformation.

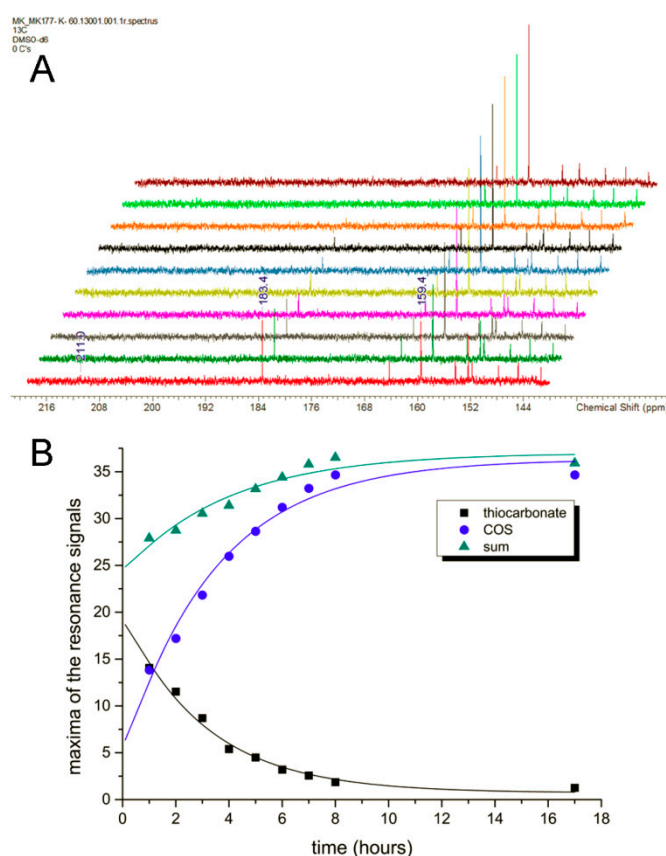


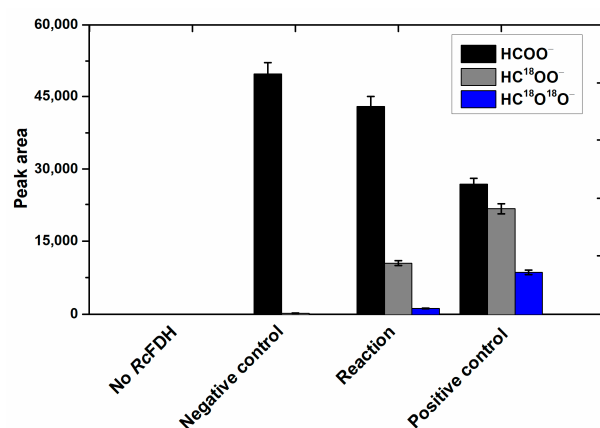
Figure 6. Time-dependent abundance of intermediate and final products of enzymatic thioformate oxidation (A) The ^{13}C NMR spectra were recorded every hour up to hour 9. The last spectrum (brown) was measured at 17 h. The resonance signal of thiocarbonate at 183.4 ppm constantly decreases, while that of COS at 159.4 ppm constantly rises. Only a small amount of the substrate (monothioformate at 211.0 ppm) is left in the first spectrum (red). (B) The development of the resonance signal maxima over time for thiocarbonate (black squares), COS (blue dots), and their sum (dark cyan triangles) shown with their respective asymptotic fits as solid lines. N.B.: the fits are not meant as proper kinetic evaluation but are added in order to approximate and visualize the development before the first collected data points and the sum of the two products. Asymptotic fits $y = a - b \times c^x$: monothiocarbonate: $a = 0.71709$ (± 0.5452); $b = -19.23708$ (± 1.01177); $c = 0.72343$ (± 0.02679); COS: $a = 36.33576$ (± 1.31434); $b = 31.7694$ (± 2.09314); $c = 0.74924$ (± 0.03287); sum: $a = 37.01988$ (± 1.04481); $b = 12.77271$ (± 1.41994); $c = 0.77727$ (± 0.05322). The experiment was carried out at 25°C and pH 9 with the enzyme bearing a minor amount of residual azide from protein preparation and with a ^{13}C -labeled thioformate substrate.

The applied concentration of the enzyme is lower than the observed abundance of monothioformate, at least in the early spectra. This implies that the primary product monothiocarbonate is able to leave the active site or even the enzyme entirely, at least under the conditions of these NMR experiments.

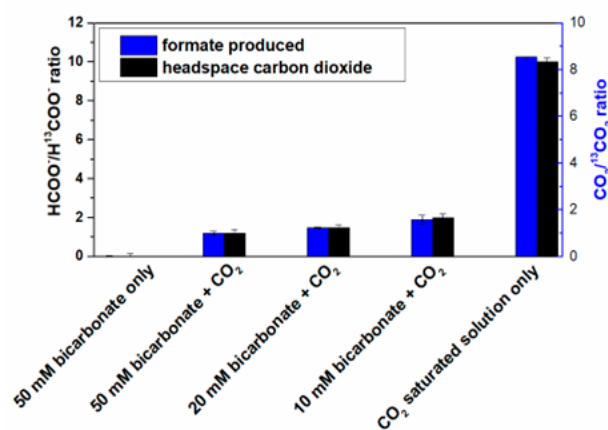
2.5. Bicarbonate Is Formed as a Direct Substrate in the Reaction of CO_2 Reduction

The results presented above show that for *R. capsulatus* FDH, bicarbonate is the final product of enzymatic formate oxidation that leaves the enzyme as such or is transformed to CO_2 in a secondary reaction within the enzyme. To determine whether CO_2 or bicarbonate are the substrates that enter the enzyme for the back reaction of CO_2 reduction, we investigated the reduction in the CO_2 substrate in more detail. Assuming that bicarbonate based on its charge cannot enter the oxidized active site through the proposed hydrophobic CO_2 channel, the formation of bicarbonate directly in the active site appears necessary, e.g.,

in a carbonic anhydrase-like reaction after CO_2 binding. Indeed, in some of the crystal structures (*D. vulgaris* Hildenborough [23], formyl-methanofuran dehydrogenase [27]), a water molecule was found attached to the conserved arginine residue close to the molybdenum/tungsten center in the active site. To analyze whether *R. capsulatus* FDH converts CO_2 to bicarbonate in the active site which is then used as a direct substrate to produce formate, we incubated the enzyme first in H_2^{18}O -labeled water, before a CO_2 saturated buffer and reduced methyl viologen were added to the mixture. After derivatization of the resultant formate with 2,3,4,5,6-pentafluoro-benzylbromide (Figure S8 in the SI), we analyzed the product with GC-MS for the presence of ^{18}O . After 10 s of the enzymatic reaction in 50% H_2^{18}O at 25 °C, the formation of formate-bearing labeled oxygen ($\text{HC}^{18}\text{O}^{16}\text{O}^-$) could indeed be verified (Figure 7a). This confirms that added CO_2 is hydrated with H_2^{18}O within the enzyme or most likely directly at the active site before its use as a substrate in the reduction to formate. In the absence of either enzyme or H_2^{18}O in the solution, no $\text{HC}^{18}\text{O}^{16}\text{O}^-$ was detected (Figure 7a). In another control reaction, H_2^{18}O was first incubated with a CO_2 -saturated buffer for 30 min to yield $\text{C}^{16}\text{O}^{18}\text{O}$ in the secondary non-enzymatic hydration of $^{12}\text{CO}_2$ before FDH was added. In this case, both $\text{HC}^{18}\text{O}^{16}\text{O}^-$ and $\text{HC}^{18}\text{O}^{18}\text{O}^-$ were detected as enzyme products (Figure 7a). Formate standard in the absence of enzyme incubated with H_2^{18}O did not show any formation of $\text{HC}^{18}\text{O}^{16}\text{O}^-$ (data not shown in Figure 7). It can, therefore, be excluded that formate exchanges oxygen atoms with water spontaneously in a non-enzymatic/non-catalyzed reaction.



(a)



(b)

Figure 7. Cont.

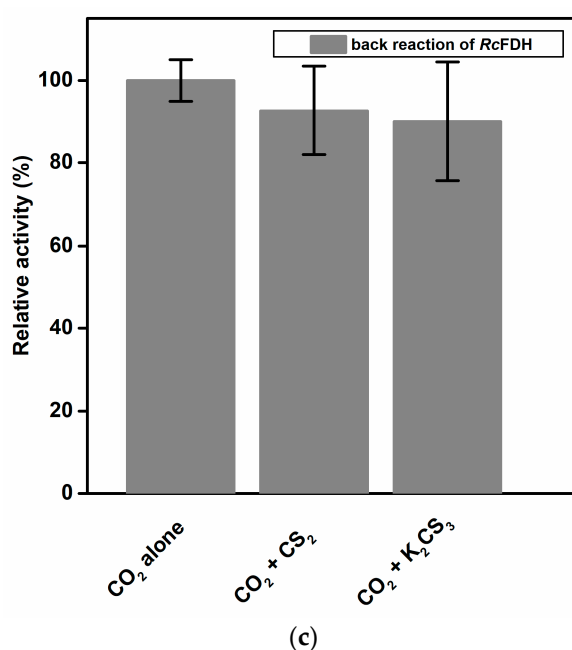


Figure 7. (a) CO₂ reduction reaction of RCFDH in the presence of H₂¹⁸O. Reaction mixture of 100 μL contained 2 mM reduced methyl viologen and CO₂-purged phosphate buffer (100 mM, pH 6.6). The reaction was started by adding the RCFDH (5 μM) and H₂¹⁸O (50%) mixture into the solution anaerobically at 25 °C. The negative control had no H₂¹⁸O added to it and in the case of the positive control, H₂¹⁸O and CO₂ were mixed 30 min prior to RCFDH addition. Reactions were stopped after 10 s by adding 30 μL of acetone followed by freezing in liquid nitrogen. Samples were derivatized and analyzed by GC – MS, as detailed in the Methods section. (b) The CO₂ reduction reaction of RCFDH using CO₂ and/or NaHC¹³O₃ as substrates. The reaction volume of 100 μL contained 2mM reduced methyl viologen and a CO₂ saturated phosphate buffer (100 mM, pH 6.6) with different concentrations of NaHC¹³O₃ solution. The reaction was started by adding RCFDH (5μM) anaerobically at 25 °C. Reactions were stopped after 10 s by adding 30 μL of acetone followed by freezing in liquid nitrogen. Samples were derivatized and analyzed by using GC–MS. Black bars represent the ratios of normal and ¹³C-labeled formate produced. Blue bars represent the headspace CO₂/¹³CO₂ ratios analyzed by GC – MS before the addition of RCFDH. (c) The effect of CS₂ and K₂CS₃ on the back reaction of RCFDH. A reaction volume of 100 μL contained 1mM NAD⁺ and a CO₂-saturated phosphate buffer (100 mM, pH 6.6). A total of 150 mM of carbon disulfide (CS₂) and 5 mM of potassium trithiocarbonate were added to check inhibition. The reaction was monitored at 340 nm for 1 min after adding RCFDH (5 μM) anaerobically at 25 °C.

In order to identify the substrate species for the reduction which enters the active site, we mixed different ratios of labeled NaH¹³CO₃ (at high pH) and unlabeled CO₂ purged buffer (at low pH) solutions as substrates and analyzed the formate isotope that was enzymatically formed by RCFDH within the first 10 s of the reaction (Figure 7b). Assuming a negligible non-enzymatic hydration of CO₂ within the first 10 s, unlabeled formate as a major product indicates that CO₂ entered the active site much more efficiently than the ¹³C-labeled bicarbonate or even exclusively under the experimental conditions. In contrast, finding ¹³C-labeled formate as a major product would have indicated that bicarbonate entered the active site preferentially. We observed relatively higher amounts of ¹²C formate (Figure 7b), indicating that a substrate entered the enzyme mostly in the ¹²CO₂ form and not as H¹³CO₃[−]. We also looked at the headspace CO₂/C¹³O₂ ratio of the reaction in a separate experiment to simulate the conditions of the period in time when the enzyme was added. These ratios correlate quite well with the formate product carbon isotope ratios indicating that the gaseous form of a substrate enters the enzyme (Figure 7b).

It is further shown that neither trithiocarbonate nor CS₂ were used as substrates for the back reaction. Likely, trithiocarbonate, like bicarbonate, cannot enter the active site

through the hydrophobic channel. Since CO₂ is apparently converted to bicarbonate in the active site in a carbonic anhydrase-like reaction, it is unsurprising that CS₂ cannot be used as a substrate because the hydration of CS₂ is substantially slower, while it evidently does interfere with the active site and/or the hydrophobic channel and, therefore, inhibits the reduction in CO₂ when present (Figure 7c).

3. Discussion

CO₂ is a kinetically and thermodynamically stable molecule, with a high negative reduction potential value for the CO₂/HCOOH pair (highly pH dependent), all of which render its activation and reduction difficult tasks [1]. For the biological reversible conversion of CO₂ to formate, prokaryotes and eukaryotes use FDH enzymes [2,3]. FDHs are a heterogeneous and broadly distributed group of enzymes that evolved to be part of diverse metabolic pathways, most notably the generation of energy from formate oxidation by coupling it to the reduction in several terminal electron acceptors, or the reduction in CO₂ into formate catalyzed by some prokaryotic organisms. FDHs belong to two major classes, the metal-dependent and the metal-independent ones [9]. The metal-dependent ones are only present in prokaryotes and were shown to catalyze the oxidation of formate with higher catalytic efficiencies as compared to the metal-independent enzymes [13]. In particular, metal-dependent enzymes are much better catalysts for the reduction in CO₂, and for a long time it was believed that metal-independent enzymes are not even able to catalyze the back reaction [10]. Metal-dependent enzymes belong to the class of Mo- or W-containing enzymes bearing the bis-MGD cofactor [11]. This class of Mo- and W-containing enzymes was first shown by Holm and coworkers in the 1980s to catalyze classical oxygen atom transfer (OAT) reactions [42]. In OATs, the oxygen atom from water is transferred to the substrate which is oxidized, or in the opposite direction, from the substrate to yield water; these reactions are coupled to the reversible transfer of two electrons and two protons in the course of the transformation cycles [22]. The electrons are directly transferred to the Mo/W metal ion of the cofactor and the metals cycle between the Mo/W^{IV} and Mo/W^{VI} oxidation states, with Mo/W^V as the intermediate state. FDH enzymes were considered to be an exception in the group of molybdenum- and tungsten-containing enzymes for catalyzing direct hydride abstraction from the parent carbon atom instead of an oxygen atom transfer [2,13,18,21]. Such exceptional behavior was mainly proposed based on a report by Khangulov et al. in 1998 [21], concluding that the immediate product of formate oxidation is CO₂ and not bicarbonate. They used an experimental setup with ¹⁸O-labeled water and ¹³C-labeled formate and observed only ¹³C¹⁶O₂ as an initial product of the reaction. This experiment and its outcome have never really been questioned since and resulted in the proposal of numerous mechanisms for FDH-catalyzed formate oxidation without considering any OAT transitions [2,10]. However, a uniformly accepted, undisputed reaction mechanism has not been put forward as of yet. Since the enzyme in the Khangulov et al. experiment was inhibited by relatively high amounts of azide [21], which was used to slow down the reaction, we decided to reinvestigate the experiment in the absence of azide. We used *R. capsulatus* FDH instead of *E. coli* FDH, an enzyme that we characterized in detail before and which is much more oxygen-tolerant compared to the *E. coli* FdhF enzyme [17]. This enabled us to use low/no azide concentrations with the enzyme for the experiments. We performed the formate oxidation assay at 10 °C to particularly slow down the secondary reaction of non-enzymatic CO₂ hydration [24]. Our data clearly show that after a reaction time of 10 s, labeled ¹³C¹⁸O¹⁶O was readily detectable, demonstrating that the oxygen of H₂¹⁸O water is, in fact, inserted into the product. The enzyme-catalyzed reaction was much faster as compared to the secondary hydration of CO₂ under our experimental conditions, as evidenced by respective control reactions.

We further show solvent kinetic isotope effects on the reactions using D₂O, H₂¹⁸O, and DCOO⁻, confirming the impact of water on the substrate transformation rates and, therefore, a mechanistic role of H₂O. It has been shown previously that the D of DCOO⁻ of formate is transferred to the sulfido ligand on the Mo-centre [15,30,32], with which

our results are entirely in accordance. To accurately determine the rate-limiting step of the reaction, more detailed investigations will be necessary during future studies. In our experimental setup, we worked with a 50% H₂¹⁸O saturated buffer which reliably gave rise to the observed solvent kinetic isotope effect.

To further confirm the insertion of oxygen into H¹³COO⁻-labeled formate and to determine the formed product intermediate, we used NMR as a detection method. Since the reaction was too fast and the ¹³C-NMR measurements were relatively time-intensive, we had to slow down the reaction with azide. The reaction was further performed at 5 °C to also decelerate the non-enzymatic hydration of CO₂. The first product that was detected by NMR in substantial abundance was bicarbonate, the formation of which already began to decrease before the abundance of CO₂ increased up to its maximum reaching even an oversaturation of the solution. In a previous report, the same observations were made, detecting bicarbonate as the first intermediate by NMR [43]. The first data point, however, was drawn only after 25 min, which impedes disentangling the still quite fast enzymatic reaction and the subsequent secondary reaction of the CO₂/HCO₃⁻ equilibrium at pH 9.0. Therefore, in order to receive even more coherent data, we used ¹³C-labeled thioformate in the experiment, which was shown to be a suitable substrate of *R. capsulatus* FDH in the bisubstrate kinetic experiments. When ¹³C-labeled thioformate was used in the NMR experiment with low azide concentrations (remnants of protein preparation), thiocarbonate was clearly detected as the first intermediate, the abundance of which then decreased while COS abundance increased steadily. Here, thiocarbonate is detected instead of thiobicarbonate, based on the fact that thiobicarbonate is more acidic than bicarbonate, less stable at this pH, and easily deprotonated. This clearly confirms the oxygen atom transfer with bicarbonate/thiocarbonate as reaction intermediates of the reaction, before CO₂ or COS are formed in a secondary follow-up reaction inside the enzyme and/or a non-enzymatic secondary reaction outside the enzyme. We further investigated the back reaction of CO₂ reduction to clarify whether bicarbonate enters the enzyme (preferentially) or whether CO₂ does instead, followed by bicarbonate formation at the active site. Using a ¹²CO₂ saturated buffer in the presence of a H₂¹⁸O saturated enzyme, we obtained H¹²C¹⁸O¹⁶O⁻-labeled formate in the first 10 s of the reaction, showing that CO₂ is the primary substrate that enters the enzyme, which is then converted to a H¹²C¹⁸O¹⁶O₂ bicarbonate at the active site (possibly in a carboanhydrase-like hydration reaction). This bicarbonate is then used as the actual substrate for the reduction to formate and water. When H¹³CO₃⁻ was used as the only substrate, no ¹⁸O-labeled formate was detected. Likely, bicarbonate is not used as a direct substrate in the back reaction because it cannot enter the enzyme through the hydrophobic CO₂ channel. Or, the entrance is hindered by the histidine, since structural changes were observed in oxidized and reduced X-ray structures [26]. In the NMR experiment, using ¹³C-labeled formate, bicarbonate was detected as an immediate intermediate product and much higher in abundance than the enzyme, suggesting it may be released from the enzyme. In this reaction, an azide-inhibited enzyme was used. For carbonic anhydrase, it was reported that azide is a competitive inhibitor for bicarbonate dehydration [44], while it is a non-competitive inhibitor for CO₂ hydration. For *E. coli* FdhF, inhibition studies with azide showed that azide acts as a competitive inhibitor for formate oxidation and as a non-competitive inhibitor for the reduction in CO₂ [30], with the inhibitor being more competent toward the oxidation of formate. For *RcFDH*, it was recently shown that azide acts as a mixed-type (competitive, non-competitive) inhibitor for both formate and CO₂ [45,46]. It was concluded in the study of the *E. coli* enzyme that the inhibitors bind differently to the reduced and oxidized forms of the enzyme. Assuming a similar inhibition mechanism for azide with bicarbonate/CO₂ in *R. capsulatus* FDH, we propose that in the reaction of formate oxidation, the bicarbonate binding site is competitively blocked by azide so that the dehydration of bicarbonate is inhibited and bicarbonate is released instead of CO₂, likely through the formate channel. The formate channel might be suitable for more charged substrates, such as formate, nitrate, and bicarbonate, while the CO₂ channel is specific for CO₂ and cannot be used by

bicarbonate [25]. Redox, charge, and protonation states of the active site should all have an impact on the attraction or repulsion of charged and uncharged substrates/products. Therefore, the presence/absence of substrates, products, inhibitors, reducing, and/or oxidizing agents might have gatekeeper function(s) for either of the substrates. Further, after reduction in the enzyme with formate, conformational changes in the second coordination sphere were observed in the crystal structures of the *D. vulgaris* FDH enzyme [23] and the reinterpreted structure of the *E. coli* FdhF enzyme [47]. We, therefore, hypothesize that by the structural rearrangement in the formate reduced enzyme, the formate funnel becomes accessible for the release of bicarbonate, an exit site that is blocked by the histidine in the oxidized enzyme or inhibited enzyme. We assume that the site for CO₂ hydration and bicarbonate dehydration is close to or at the conserved arginine residue in the second coordination sphere, since in the crystal structures of the *D. vulgaris* [23] and formylmethanofuran dehydrogenase from *Methanothermobacter wolfeii* [27], a water molecule was identified to reside in the vicinity of this residue. In previous studies, it was also speculated that azide is bound to this residue in the active site, matching our hypothesis that this is the non-competitive binding site for azide and bicarbonate [32,45]. Overall, we want to propose the oxygen atom transfer mechanism for the reversible oxidation of formate by metal-containing FDH enzymes, as shown in Figure 8, which shows similarities to well-accepted enzyme mechanisms, such as the one for xanthine oxidase. We think that all metal-containing FDHs would work after this mechanism and that there are no differences in W- or SeCys-containing enzymes

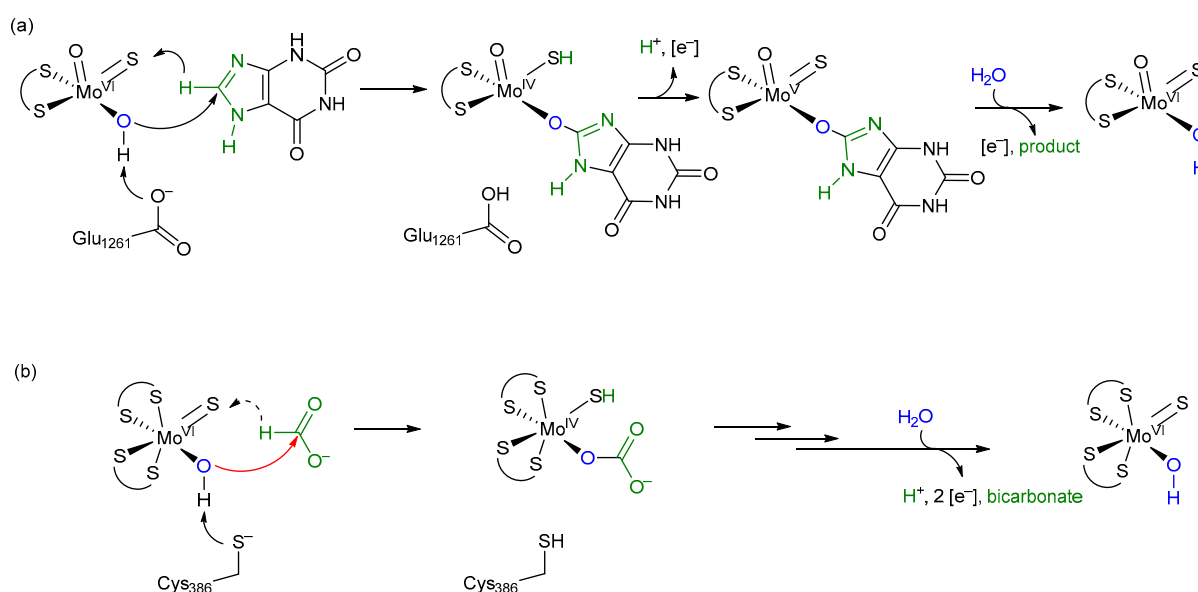


Figure 8. (a) The mechanism for xanthine oxidase adapted from Ref. [22]. (b) A tentatively proposed short mechanism for FDH operating via oxygen atom transfer. The similarity of the two substrates at the site of transformation is emphasized in green. The arrow shown in red constitutes the attack of the active site on the substrate which initiates OAT, which is immediately followed by a hydride or proton-coupled electron transfer to the sulfido ligand. In both mechanisms, the product is released (bicarbonate in the case of FDH) and water is bound to the active site.

Considering the difference between formate and xanthine at the site of enzymatic transformation being only the presence of two N functionalities versus two oxygen functionalities and a relatively similar bonding situation thereof, the oxygen atom transfer mechanism of FDH is tentatively proposed to resemble that of XO (xanthine oxidase), with the –OH groups of the initial species stemming from water [22] (Figure 8). All protonation or deprotonation states of substrates, amino acids, and ligands will be directly dependent on the concentration of protons in the active site, i.e., its pH value. For a more detailed

mechanistic insight into the actual individual transformative steps, a number of further experiments will need to be carried out.

The release of the bicarbonate product, one proton, and two electrons from the inner active site composition regenerates the species with which this cycle starts. The key step of this proposed mechanism constitutes a typical and common oxygen atom transfer, as implied by our presented new data and as proposed for xanthine oxidase. This mechanism is in accordance with all undisputed experimental data available, stoichiometrically balanced and, hence, coherent.

In our mechanism, we propose that after formate binding the amino acid ligand at the Mo atom is displaced by water, which might be facilitated by a conformational change in the enzyme upon formate binding. The displacement of the cysteine ligand in *R. capsulatus* FDH has been shown by us in previous studies by iodoacetamide labeling of the nitrate-inhibited and formate-reduced enzyme and by EXAFS studies [13,14]. The iodoacetamide labeling of the selenocysteine ligand was also shown for the *E. coli* enzyme [13]. However, not all enzymes are inhibited by iodoacetamide, e.g., the *D. vulgaris* Hildenborough enzyme [23]. In this enzyme, no carboxamidomethyl labeling of the selenocysteine ligand was observed. Notably, in this experiment, a nitrate and a glycerol-inhibited enzyme were used, and in particular glycerol might interfere with the accessibility of iodoacetamide to this enzyme [23]. Further, selenocysteine-containing enzymes are more oxygen sensitive, and it remains possible that after the displacement of the selenocysteine ligand, the selenocysteine is easily oxidized and the oxidized SeO_2 or SeO_3 species do not react with iodoacetamide. We also do not exclude that distinct FDH enzymes have different accessibility for iodoacetamide, e.g., by variations of amino acids in the formate-binding funnel. EXAFS studies of the *R. capsulatus* enzyme further proved displacement of the cysteine residue in the formate-reduced enzyme by an oxygen atom (which can be the one from water as shown in this study). In the EXAFS data of the azide or cyanate-inhibited enzyme, instead of cysteine sulfur a light atom was observed to be bound to the molybdenum center [28], which we assigned to be an oxygen atom from water rather than a C or N atom from the inhibitors which are proposed to not directly bind to molybdenum. The binding of water observed in the EXAFS studies supports our oxygen atom transfer mechanism. In contrast, for the *E. coli* FdhF and *D. vulgaris* enzymes, EXAFS and crystallographic studies did not support displacement of the selenocysteine ligand [23,48]. We consider it likely that the *E. coli* enzyme was oxidatively damaged and the sulfido ligand was lost in the enzyme preparation for the EXAFS studies, while in the formate reduced structure of the *D. vulgaris* enzyme, the oxidation state of the molybdenum atom is not clear and the crystallized enzyme might be in the re-oxidized Mo^{VI} state after product release since neither the product nor the substrate was present in the structure. Often, EPR studies are considered as an argument for the oxidation state-dependent active site structure of the enzyme. However, the Mo^{V} active site constitutes an intermediate state after product release and one electron oxidation in which the amino acid ligand is quite likely to rebind again to the molybdenum atom which otherwise would be coordinatively unsaturated [18,49]. In previous studies, several groups proposed a hydride transfer mechanism with the formate being bound within the second coordination sphere of the active site metal [15,50]. One of the arguments used by the authors to support their mechanism was that the second $\text{p}K_{\text{a}}$ value of formic acid (i.e., the one for C-H dissociation) disfavors a proton abstraction and the resulting carbanion would be unstable. In our mechanism, the formate is directly bound to the molybdenum atom through an oxido function derived from a water molecule, so a carbanion would not be formed after proton abstraction [2]. Nevertheless, in our mechanism, we leave it open whether the hydrogen of formate is transferred as a hydride or in a proton-coupled electron transfer reaction to the sulfido ligand, forming the SH group and the reduced Mo^{IV} (i.e., we do not propose the direction in which the electrons or electron pairs move when entering the transition state). The sulfido group as a hydride (or proton) acceptor has been well-established in XDH enzymes [51] and was proven in FDH enzymes by EPR studies to contain a strongly coupled, solvent exchangeable and substrate-derived proton with a

hyperfine constant of 20–30 MHz, which is consistent with the hydrogen atom from the formate being transferred to this ligand in the first coordination sphere of the molybdenum upon reduction. This observation is also consistent with our model reaction mechanism; however, it does not prove that the H-atom is transferred as a hydride.

Meneghello et al. (2021) [20] recently chose an electrochemical approach with the tungsten-containing FDH from *Desulfovibrio vulgaris* Hildenborough for confirming the substrate of FDHs for the back reaction of CO₂ reduction being CO₂ rather than HCO₃[−], as previously and repeatedly concluded before. However, we want to point out that product formation was not measured in this study and that in their experimental setup, the enzymes might have been washed away; therefore, their results need to be taken with caution. As already emphasized by Cooper et al. (1968) [24] and confirmed by our investigation, respective studies do not necessarily reflect what is happening directly at the active site. We, therefore, propose that for the reduction of CO₂ the intermediate ionic species HCO₃[−] is hindered from entering the reduced active site via the hydrophobic CO₂ channel that has been identified in crystal and cryo-EM structures, while CO₂ instead can easily enter. This is still consistent with the report by Meneghello et al. (2021) [20]. At the active site, CO₂ then reacts with H₂O to form HCO₃[−] which subsequently provides the direct substrate for the back reaction resulting in formate and water formation through oxygen atom transfer from bicarbonate. In conclusion, we also want to emphasize that mechanistic studies of metal-containing FDH enzymes need to be performed in the absence of any inhibitor under strictly anaerobic conditions.

4. Materials and Methods

4.1. Chemicals and Reagents

Elemental potassium was purchased from Sigma-Aldrich (St. Louis, MI, USA). ¹³C-labeled formic acid (¹³C, 99%) was purchased from Cambridge Isotope Laboratories, Inc. (Tewksbury, MA, USA). Phenol was purchased from Fisher Scientific (Waltham, MA, USA). POCl₃ was purchased from Acros (Geel, Belgium). Penta fluorobenzyl bromide (PFBBBr) was purchased from Alfa Aesar (Haverhill, MA, USA). Potassium hydrogenphosphate and potassium dihydrogenphosphate were purchased from Sigma-Aldrich. Potassium dithioformate was prepared according to a literature method [52].

4.2. Synthesis of Monothioformate

First, the starting materials KHS and phenyl formate had to be synthesized.

(i) Synthesis of potassium hydrogen sulfide (KHS). Potassium hydrogen sulfide, according to literature reports, is most commonly synthesized by the reaction between a solution of potassium sulfide with excess dihydrogen sulfide. However, the such-synthesized potassium hydrogen sulfide is not completely pure. To avoid water and any other impurities, the following modified procedure was used to synthesize dry and pure potassium hydrogen sulfide. A total of 12 mL of dry ethanol was charged in a pre-evacuated flask which was equipped with a stirrer and bubbler under nitrogen. The flask was cooled to −78 °C (a mixture of isopropanol and liquid nitrogen was used as a cooling bath). Then, 1.7 g of potassium was inserted into the flask gradually and cautiously in small portions over a period of 2 h. When all of the potassium particles had dissolved, dry gaseous dihydrogen sulfide which was produced through a Kipps apparatus and dried over CaCl₂, which was passed through the reaction mixture for about 4 h. As soon as the passing of dihydrogen sulfide started, the formation of a white precipitate could be observed. The passing of dihydrogen sulfide was continued until the end of precipitation. Then, the excess gaseous dihydrogen sulfide was removed by bubbling nitrogen through the solution. The solid compound was dried under a vacuum for 3 h. Elemental analysis (calcd). S 44.43, H 1.397; found S 43.11, H 1.80; IR (KBr): ν cm^{−1} = 2520 (w), 2100 (br), 1650 (s), 1400 (br), 1250 (w), 1150 (m), 1000 (s), and 700 (w).

(ii) Phenyl formate was synthesized with small modifications to a literature procedure [53]. A total of 1.2 eq of ¹³C-labeled formic acid (21.2 mmol, 0.975 g) was mixed with

1 eq of phenol (17.67 mmol, 1.66 g) in a three-neck round bottom flask under a nitrogen atmosphere. The reaction mixture was stirred for 3 h at 80 °C under nitrogen. Then, the reaction mixture was cooled to room temperature and 0.33 eq of POCl₃ (5.83 mmol, 0.89 g) was added slowly and dropwise. The reaction mixture was poured slowly into a solution of sodium bicarbonate in ice water. The resultant solution was then extracted three times with diethyl ether (40 mL). The combined organic phases were dried over sodium sulfate, filtered, and the solvent was removed from the filtrate with a rotary evaporator at a low temperature to obtain crude phenyl formate. Phenyl formate is not stable and should be used immediately for the following step. ¹HNMR (CDCl₃, 400MHz, 298 K): δ: 8.37 ppm (1H, CH), δ: 7.43 ppm (2H, CH-Ar), δ: 7.26 ppm (1H, CH-Ar), δ: 7.07 ppm (2H, CH-Ar); ¹³CNMR (CDCl₃, 400MHz, 298 K): δ: 161.12 ppm (1C, CH), δ: 155.54 ppm (1C, C), δ: 115.75 ppm (2C, CH), δ: 130 ppm (2C, CH), and δ: 121.10 ppm (C, CH).

(iii) Potassium monothioformate was synthesized with small modifications to a literature procedure. A total of 1 eq of phenyl formate (18 mmol, 2.20 g) was mixed with 1 eq of dry KHS (18 mmol, 1.30 g) in a Schlenk flask under nitrogen. The Schlenk flask was placed into an ultrasonic bath at 0 °C for 2 h. Then, 2 mL of dry methanol was added to the Schlenk flask and the mixture was stirred for another 2 h. After the addition of 20 mL of dry diethyl ether, the reaction mixture started to form a precipitate. After precipitation stopped, anaerobic filtration was carried out under a nitrogen atmosphere. The precipitate was washed with small amounts of cold methanol and dried under a vacuum to yield a fine pale yellow powder. ¹HNMR (CDCl₃, 400MHz, 298 K): δ: 9.8 ppm and δ: 10.4 ppm (1H, CH) and ¹³CNMR (CDCl₃, 400MHz, 298 K): δ: 211.11 ppm (1C, CH). Two resonances were detected due to the tautomerization effect. MS (ESI): *m/z* = 101.4 [M] H¹³COSK. IR (KBr): ν_{max} = 2580 (C-H stretching), 1630 (C=O stretching), 1390 (C-H bending), 812 (C-S). Elemental analysis (calcd). C 11.99, H 1.01, and S 32.00; found C 11.96 and H 1.54; S 31.41.

4.3. NMR Spectroscopy

NMR spectra were recorded on a Bruker Avance II 300 spectrometer (300, 75, and 121.5 MHz, respectively). Chemical shifts (δ) are given in parts per million (ppm) using solvent signals as a reference (DMSO-d₆ ¹H: δ = 2.50 ppm; ¹³C: δ = 39.52 ppm; CD₃OD ¹H: δ = 3.31 ppm; ¹³C: δ = 49.15 ppm) relative to external tetramethylsilane (δ = 0 ppm).

4.4. Preparation of the Time-Dependent NMR Measurement Sample for the Enzymatic Reaction of RCFDH with ¹³C-Labeled Sodium Formate

In order to prepare the nicotinamadeninucleotide stock (150 mM), 99.5 mg of NAD⁺ was dissolved in 1 mL of a tris(hydroxymethyl)aminomethane buffer (75 mM, pH: 9). For preparing the sodium azide stock (50 mM), 3.25 mg of sodium azide was dissolved in 1 mL of a buffer. After the preparation of the stocks, 290 μL of NAD⁺ stock was charged in a new vial. Then, 100 μL of labeled sodium formate (1.62 M; 11.2 mg in buffer at pH 9), 24 μL of sodium azide, and 150 μL of a buffer were added, respectively. Finally, and immediately before the NMR measurement series started, 60 μL of an enzyme (360 μM; for preparation see below) was inserted into the reaction mixture. A total of 0.5 mL of the prepared mixture was transferred quickly to the NMR tube. Deuterated methanol (CD₃OD) was used as the internal standard in an insert tube (i.e., not mixed with the sample solution). The ¹³C time-dependent measurements were started immediately without filtration of the sample at 5 °C and run in automation overnight.

4.5. Preparation of the Time-Dependent NMR Measurement Sample for the Enzymatic Reaction of RCFDH with a ¹³C-Labeled Monothioformate

NAD⁺ stock solution was prepared as described above. A total of 290 μL of NAD⁺ stock was charged in a new vial. Then, 100 μL of monothioformate (1.12 M; 11.2 mg in buffer at pH 9) and 150 μL of water were added. Finally, 60 μL of an enzyme (360 μM) was added to the sample mixture immediately before the measurements started. A total of 0.5 mL of the prepared mixture was transferred quickly to the NMR tube. Deuterated DMSO-d₆

(dimethylsulfoxide) was used as the internal standard in an insert tube (i.e., not mixed with the sample solution). The ^{13}C time-dependent measurements were started immediately without filtration of the sample solution at room temperature (25 °C operation temperature in the NMR laboratory) allowing for continuous monitoring of the transformations.

4.6. Control Measurements for the Thioformate Substrate Series

The same procedure as described above was followed with regard to sample preparation, except that one component or more were left out (Table 4). The total volume of the reaction mixture was 600 μL in all cases, of which 5 mL was transferred to the NMR tube. The solution volume with the ingredient not included in the control mixture was replaced by the buffer to reach the total volume of 600 μL .

Table 4. Overview of sample composition for the control NMR experiments.

| Control Reaction | VEnzyme (μL) | VNAD+ (μL) | VSubstrate (Monothioformate) (μL) | Buffer (pH 9) (μL) |
|------------------|---------------------------|-------------------------|--|---------------------------------|
| a | 0 | 290 | 100 | 210 |
| b | 60 | 0 | 100 | 440 |
| c | 60 | 290 | 0 | 250 |
| d | 0 | 290 | 0 | 310 |
| e | 0 | 0 | 0 | 600 |

a, control reaction without an enzyme (RcFDH); b, control reaction without NAD⁺; c, control reaction without a substrate (monothioformate); d, control reaction without an enzyme (RcFDH) and a substrate (monothioformate); e, control reaction without substrate (monothioformate) and NAD⁺.

In none of the control condition experiments could any progress of the enzymatic reaction be observed. The resonances at 183.4 ppm for thiocarbonate and 159.4 ppm for COS remained absent. Although NAD⁺ has many ^{13}C -NMR signals in a broad range of the spectrum, these do not interfere with the signals of the enzymatic transformation of interest. In contrast to all other components of the reaction, FDH enzyme concentration is so low that no respective signals could be observed. Tris(hydroxymethyl)aminomethane (THAM) was used for the preparation of the buffer (pH = 9), which has two resonances in the ^{13}C -NMR spectrum (56.14 ppm and 61.92 ppm). An additional coupling ^{13}C -measurement (4 h duration) for the reaction mixture bearing all components proved that the intermediate at 183.4 ppm is not showing any splitting in the ^{13}C {H} coupled NMR. This means that there is no proton in scalar coupling with this carbon atom, which further supports an assignment to the thiocarbonate dianion (Figure S5).

4.7. The Expression and Purification of *R. capsulatus* FDH

R. capsulatus FDH was expressed in *E. coli* MC1061 cells containing plasmids pTHfds05 and pTHfds07 obtained from a previous study [17] and purified according to the published procedure [25]. The enzyme was stored in a 75 mM Kpi buffer containing 10 mM sodium azide, pH 7.5, and before usage of the enzyme in the assays, the buffer was exchanged with a 75 mM Kpi buffer, pH 7.5, using PD-10 desalting columns (Sephadex G-25 M; Amersham Biosciences) to remove azide.

4.8. ^{13}C -Labeled Formate Oxidation by RcFDH in the Presence of ^{18}O -Labeled Water

The oxidation of ^{13}C -labeled formate by RcFDH in the presence of ^{18}O -labeled water was carried out to analyze the resultant CO₂ isotope composition. The reaction mixture of 100 μL was prepared in a glass insert containing a GC vial by mixing 10 mM ^{13}C -labeled formate and 5 mM NAD⁺ anaerobically in 100 mM Tris-HCl, pH 9. *R. capsulatus* FDH, pre-mixed with ^{18}O -labeled water, was anaerobically transferred to a syringe. The final concentration of the enzyme and ^{18}O -containing water were 10–30 μM and 10–50%, respectively. The reaction was started by injecting the assay mixture into the closed GC

vial at 10 °C. For control reactions, up to 100 mM NaH¹³CO₃ was used as a ¹³CO₂ source. All the reagents were pre-incubated at the required temperatures beforehand. Headspace samples were taken from the vial by the autosampler after the indicated time intervals. The isotopic composition of produced ¹³CO₂ was analyzed by using GC-MS QP2010 SE (Schimadzu) modified for headspace samples. Sample volumes of 1–5 µL were used in the DB-WAX UI column (30 m × 0.32 mm × 0.25 µm, Agilent). The injection temperature was kept at 200 °C. The temperature program for analysis consisted of (i) 30 °C for 3 min; (ii) from 30 °C to 200 °C at 30 °C/min; (iii) 200 °C for 1 min; and (iv) from 200 °C to 30 °C at 30 °C/min.

For MS analysis, the selected ion monitoring (SIM) mode was used due to its high sensitivity. A detector voltage of +0.3 kV relative to tuning with the ion source and interface temperature of 200 °C was applied each. The MS analysis method was used to look for *m/z* values corresponding to the ¹³C¹⁶O¹⁶O, ¹³C¹⁶O¹⁸O, and C¹³O¹⁸O¹⁸ isotopomers of CO₂. Different concentrations of NaH¹³CO₃ solutions were used to confirm the correct *m/z* values and to create a calibration curve (Figure S9).

4.9. Derivatization and Analysis of the Formate Using GC-MS

The formate was derivatized by modifying a previous method [54] using 2,3,4,5,6-pentafluoro-benzylbromide (PFBBBr). A total of 100 µL of enzyme-free samples were mixed with 50 µL of a 325 mM phosphate buffer, pH 8.5. To this, 365 µL of 100 mM PFBBBr solution prepared in acetone was added. The solution was vortexed for 1 min and heated at 60 °C for 20 min. After cooling down to room temperature, 500 µL of *n*-hexane was added and vortexed for 1 min. Phases were separated by centrifugation at 13,000 rpm for 1 min and the upper organic phase was carefully pipetted into a 2 mL insert containing GC vials. The samples were analyzed by using GC-MS QP2010 SE (Schimadzu) modified for headspace samples. Sample volumes of 1 µL were used in the DB-WAX UI column (30 m × 0.32 mm × 0.25 µm, Agilent).

4.10. The Solvent Kinetic Isotope Effect Using Pre-Steady State Kinetics

The solvent kinetic isotope effect for the reductive half-reaction was studied using deuterated water (D₂O) in comparison to H₂O. An SX-20 stopped-flow spectrophotometer (Applied Photophysics, Inc., Leatherhead, UK) was used to study the reaction of the formate using purified *R. capsulatus* FDH. A total of 5 µM of FDH was anaerobically equilibrated in a 100 mM Kpi buffer, pH/pD = 7.9, to remove the azide present from the purification. pD of the deuterated buffer was adjusted 0.4 units higher in the pH meter (pD = pH + 0.4). Glucose oxidase (10 IU) and catalase (100 IU) were mixed with enzymes to remove the residual oxygen from the stopped-flow cell. The preparation was filled into a 10 mL glass syringe anaerobically. The second syringe was filled with the anaerobically prepared formate or deuterated formate solution (5 mM) in the same buffer and was containing 5 mM glucose. Since the stopped-flow instrument was not in an anaerobic chamber, additional modifications from Applied Photophysics, Inc. were adopted. Additional nitrogen was continuously purged around the syringe housings of the instrument. The water bath was purged with nitrogen for 30 min to remove oxygen. Both photomultiplier tube (PMT) and photodiode array (PDA) detectors were used alternatively depending on the type of experiment. The path length used for the experiments, unless mentioned otherwise, was 1 cm. The reaction of the formate with as-isolated *R. capsulatus* FDH was performed as described by Niks et al. (2016) [15] at 10 °C. The formate was used at saturating concentrations and enzyme concentrations used were between 2.5–15 µM, depending on the experiment. In the case of the PMT detector, changes at 450 nm were followed. In the case of the PDA detector, spectra were recorded between 280–700 nm wavelengths. The curves obtained at 450 nm were fitted to the sum of three exponentials using non-linear least square regression analysis using the following equation:

$$A_t = A_\infty \pm \sum A_n \exp\left(-\frac{t}{k_n}\right)$$

where n represents the number of kinetic phases. Data analysis was performed using ProData Viewer 4.2.0 (Applied Photophysics, Inc.).

4.11. The Solvent Kinetic Isotope Effect at Different pH Values

The effect of solvent isotopes (D_2O and $H_2^{18}O$) at different pH was determined anaerobically by following the formation of NADH at 340 nm. A 100 mM phosphate buffer was used at pH values between 6.0 and 7.5 and a 100 mM Tris HCl buffer was used at pH values between 8.0 and 9.0. A D_2O/H_2O or $H_2^{18}O/H_2O$ ratio of 0.5 was chosen for all the measurements by adding 50% D_2O , $H_2^{18}O$, or H_2O to the assay mixture. The reaction volume of 100 μ L contained 10 mM of formate, 2 mM NAD^+ , and the indicated buffer. The reaction was started by adding 25 nM FDH to the cuvette, followed by photometric detection at 340 nm for 60 s.

4.12. Steady State Kinetics

RcFDH kinetic assays were measured anaerobically using a UV-2401PC spectrophotometer (Shimadzu Europa, Duisburg, Germany) and following the formation of NADH at 340 nm ($\epsilon_{NADH} = 6220 \text{ m}^{-1} \cdot \text{cm}^{-1}$). Steady state kinetics for monothioformate were determined by varying the concentrations of monothioformate (0.5–20mM) and NAD (0.05–2mM). In the case of formate, the concentration varied both for formate and NAD and was 0.05–2mM. The assay was always started with the addition of RcFDH (4–8 nM) and the NADH formation was monitored for 60 s. Data obtained were fitted with the Hill function ($[y = V_{max} \times X^n / (K_{mn} + X^n)]$, $n = 1$) and Origin software (OriginPro 8.1G SR1; OriginLab Corporation, Northampton, MA, USA).

Supplementary Materials: The following supporting information can be downloaded at <https://www.mdpi.com/article/10.3390/molecules28041537/s1>, Figure S1. ^{13}C NMR spectrum depicting formate (171.3 ppm), bicarbonate (161.1 ppm), and CO_2 (125.5 ppm) signals. Figure S2. $^{13}C\{^1H\}$ NMR spectrum confirming the C-H association of formate (170.3, 172.7 ppm). Figure S3. ^{13}C NMR example spectrum of the thioformate experiment. Figure S4. ^{13}C NMR spectrum of the thioformate reaction mixture after 32 h. Figure S5. $^{13}C\{^1H\}$ NMR spectrum of the thioformate reaction mixture recorded after 32 h. Figure S6. ^{13}C NMR spectrum of $NaHCO_3$ salt in a buffer at pH 9 at room temperature without enzyme. Figure S7. The control experiment with CO_2 (unlabeled) dissolved directly into a buffer solution without enzyme and without NAD^+ . Figure S8. Time-dependent series of NMR spectra for the enzymatic conversion of formate. Figure S9. Calibration curve for the 2,3,4,5,6-pentafluoro-benzylbromide (PFBBBr)-derivatized formate. Figure S10. Calibration curve for $^{13}CO_2$ by using different concentrations of $NaH^{13}CO_3$ at pH 9.0.

Author Contributions: H.K. performed the enzyme purification and kinetic analyses. M.K. and S.S.M.B. performed the NMR analyses. Project conception and overall supervision were provided by S.L. and C.S., S.L., C.S., H.K. and M.K. wrote the manuscript. All authors have read and agreed to the published version of the manuscript.

Funding: This work was supported by the DFG under Germany's Excellence Strategies—EXC 314/2 EXC 2008/1 (UniSysCat) (S.L.). It was funded by the Deutsche Forschungsgemeinschaft (DFG, German Research Foundation) under Germany's Excellence Strategy—EXC 2008—390540038—UniSysCat. DFG-SPP 1927 grants (LE1171/15-2) and (SCHU 1480/4-2; to C.S.) were funded by the Deutsche Forschungsgemeinschaft (DFG, German Research Foundation).

Institutional Review Board Statement: Not applicable.

Informed Consent Statement: Not applicable.

Data Availability Statement: Not applicable.

Acknowledgments: We thank Benjamin Duffus (Potsdam University) for helpful discussions and suggestions.

Conflicts of Interest: The authors declare no conflict of interest.

Sample Availability: Samples of the compounds are available from the authors.

References

1. Appel, A.M.; Bercaw, J.E.; Bocarsly, A.B.; Dobbek, H.; Dubois, D.L.; Dupuis, M.; Ferry, J.G.; Fujita, E.; Hille, R.; Kenis, P.J.; et al. Frontiers, Opportunities, and Challenges in Biochemical and Chemical Catalysis of CO₂ Fixation. *Chem. Rev.* **2013**, *113*, 6621–6658. [[CrossRef](#)] [[PubMed](#)]
2. Maia, L.B.; Moura, I.; Moura, J.J.G. Carbon dioxide utilization—the formate route. In *Enzymes for Solving Humankind's Problems*; Springer: Berlin, Germany, 2021; pp. 29–81.
3. Hartmann, T.; Schwanzhold, N.; Leimkuhler, S. Assembly and catalysis of molybdenum or tungsten-containing formate dehydrogenases from bacteria. *Biochim. Biophys. Acta* **2015**, *1854*, 1090–1100. [[CrossRef](#)] [[PubMed](#)]
4. Miller, M.; Robinson, W.E.; Oliveira, A.R.; Heidary, N.; Kornienko, N.; Warnan, J.; Pereira, I.A.C.; Reisner, E. Interfacing Formate Dehydrogenase with Metal Oxides for the Reversible Electrocatalysis and Solar-Driven Reduction of Carbon Dioxide. *Angew. Chem. Int. Ed. Engl.* **2019**, *58*, 4601–4605. [[CrossRef](#)] [[PubMed](#)]
5. An, L.; Chen, R. Direct formate fuel cells: A review. *J. Power Sources* **2016**, *320*, 127–139. [[CrossRef](#)]
6. Schuchmann, K.; Müller, V. Direct and reversible hydrogenation of CO₂ to formate by a bacterial carbon dioxide reductase. *Science* **2013**, *342*, 1382–1385. [[CrossRef](#)]
7. Sokol, N.W.; Sanderman, J.; Bradford, M.A. Pathways of mineral-associated soil organic matter formation: Integrating the role of plant carbon source, chemistry, and point of entry. *Glob. Chang. Biol.* **2019**, *25*, 12–24. [[CrossRef](#)]
8. Maia, L.B.; Fonseca, L.; Moura, I.; Moura, J.J. Reduction of Carbon Dioxide by a Molybdenum-Containing Formate Dehydrogenase: A Kinetic and Mechanistic Study. *J. Am. Chem. Soc.* **2016**, *138*, 8834–8846. [[CrossRef](#)]
9. Nielsen, C.F.; Lange, L.; Meyer, A.S. Classification and enzyme kinetics of formate dehydrogenases for biomanufacturing via CO₂ utilization. *Biotechnol. Adv.* **2019**, *37*, 107408. [[CrossRef](#)]
10. Niks, D.; Hille, R. Reductive activation of CO₂ by formate dehydrogenases. *Methods Enzymol.* **2018**, *613*, 277–295. [[CrossRef](#)]
11. Hille, R. The mononuclear molybdenum enzymes. *Chem. Rev.* **1996**, *96*, 2757–2816. [[CrossRef](#)]
12. Boyington, J.C.; Gladyshev, V.N.; Khangulov, S.V.; Stadtman, T.C.; Sun, P.D. Crystal structure of formate dehydrogenase H: Catalysis involving Mo, molybdopterin, selenocysteine, and an Fe₄S₄ cluster. *Science* **1997**, *275*, 1305–1308. [[CrossRef](#)] [[PubMed](#)]
13. Hartmann, T.; Schrapers, P.; Utesch, T.; Nimtz, M.; Rippers, Y.; Dau, H.; Mroginski, M.A.; Haumann, M.; Leimkuhler, S. The Molybdenum Active Site of Formate Dehydrogenase Is Capable of Catalyzing C-H Bond Cleavage and Oxygen Atom Transfer Reactions. *Biochemistry* **2016**, *55*, 2381–2389. [[CrossRef](#)] [[PubMed](#)]
14. Schrapers, P.; Hartmann, T.; Kositzki, R.; Dau, H.; Reschke, S.; Schulzke, C.; Leimkuhler, S.; Haumann, M. Sulfido and cysteine ligation changes at the molybdenum cofactor during substrate conversion by formate dehydrogenase (FDH) from *Rhodobacter capsulatus*. *Inorg. Chem.* **2015**, *54*, 3260–3271. [[CrossRef](#)]
15. Niks, D.; Duvvuru, J.; Escalona, M.; Hille, R. Spectroscopic and Kinetic Properties of the Molybdenum-containing, NAD⁺-dependent Formate Dehydrogenase from *Ralstonia eutropha*. *J. Biol. Chem.* **2016**, *291*, 1162–1174. [[CrossRef](#)] [[PubMed](#)]
16. Niks, D.; Hille, R. Molybdenum- and tungsten-containing formate dehydrogenases and formylmethanofuran dehydrogenases: Structure, mechanism, and cofactor insertion. *Protein Sci.* **2019**, *28*, 111–122. [[CrossRef](#)] [[PubMed](#)]
17. Hartmann, T.; Leimkuhler, S. The oxygen-tolerant and NAD-dependent formate dehydrogenase from *Rhodobacter capsulatus* is able to catalyze the reduction of CO₂ to formate. *FEBS J.* **2013**, *280*, 6083–6096. [[CrossRef](#)] [[PubMed](#)]
18. Maia, L.B.; Moura, J.J.; Moura, I. Molybdenum and tungsten-dependent formate dehydrogenases. *J. Biol. Inorg. Chem.* **2015**, *20*, 287–309. [[CrossRef](#)]
19. Thauer, R.K.; Kaufer, B.; Fuchs, G. The active species of 'CO₂' utilized by reduced ferredoxin:CO₂ oxidoreductase from *Clostridium pasteurianum*. *Eur. J. Biochem.* **1975**, *55*, 111–117. [[CrossRef](#)]
20. Meneghello, M.; Oliveira, A.R.; Jacq-Bailly, A.; Pereira, I.A.C.; Leger, C.; Fourmond, V. Formate Dehydrogenases Reduce CO₂ Rather than HCO₃[−]: An Electrochemical Demonstration. *Angew. Chem. Int. Ed. Engl.* **2021**, *60*, 9964–9967. [[CrossRef](#)]
21. Khangulov, S.V.; Gladyshev, V.N.; Dismukes, G.C.; Stadtman, T.C. Selenium-containing formate dehydrogenase H from *Escherichia coli*: A molybdopterin enzyme that catalyzes formate oxidation without oxygen transfer. *Biochemistry* **1998**, *37*, 3518–3528. [[CrossRef](#)]
22. Hille, R.; Hall, J.; Basu, P. The mononuclear molybdenum enzymes. *Chem. Rev.* **2014**, *114*, 3963–4038. [[CrossRef](#)] [[PubMed](#)]
23. Oliveira, A.R.; Mota, C.; Mourato, C.; Domingos, R.M.; Santos, M.F.A.; Gesto, D.; Guigliarelli, B.; Santos-Silva, T.; Romão, M.J.; Pereira, I.A.C. Toward the Mechanistic Understanding of Enzymatic CO₂ Reduction. *ACS Catal.* **2020**, *10*, 3844–3856. [[CrossRef](#)]
24. Cooper, T.G.; Tchen, T.T.; Wood, H.G.; Benedict, C.R. The carboxylation of phosphoenolpyruvate and pyruvate. I. The active species of "CO₂" utilized by phosphoenolpyruvate carboxykinase, carboxytransphosphorylase, and pyruvate carboxylase. *J. Biol. Chem.* **1968**, *243*, 3857–3863. [[CrossRef](#)] [[PubMed](#)]
25. Radon, C.; Mittelstadt, G.; Duffus, B.R.; Burger, J.; Hartmann, T.; Mielke, T.; Teutloff, C.; Leimkuhler, S.; Wendler, P. Cryo-EM structures reveal intricate Fe-S cluster arrangement and charging in *Rhodobacter capsulatus* formate dehydrogenase. *Nat. Commun.* **2020**, *11*, 1912. [[CrossRef](#)] [[PubMed](#)]
26. Vilela-Alves, G.; Manuel, R.R.; Oliveira, A.R.; Pereira, I.C.; Romão, M.J.; Mota, C. Tracking W-Formate Dehydrogenase Structural Changes During Catalysis and Enzyme Reoxidation. *Int. J. Mol. Sci.* **2022**, *24*, 476. [[CrossRef](#)]
27. Wagner, T.; Ermler, U.; Shima, S. The methanogenic CO₂ reducing-and-fixing enzyme is bifunctional and contains 46 [4Fe-4S] clusters. *Science* **2016**, *354*, 114–117. [[CrossRef](#)]

28. Duffus, B.R.; Schrapers, P.; Schuth, N.; Mebs, S.; Dau, H.; Leimkuhler, S.; Haumann, M. Anion Binding and Oxidative Modification at the Molybdenum Cofactor of Formate Dehydrogenase from *Rhodobacter capsulatus* Studied by X-ray Absorption Spectroscopy. *Inorg. Chem.* **2020**, *59*, 214–225. [[CrossRef](#)]
29. Zou, Y.; Zhang, H.; Brunzelle, J.S.; Johannes, T.W.; Woodyer, R.; Hung, J.E.; Nair, N.; van der Donk, W.A.; Zhao, H.; Nair, S.K. Crystal structures of phosphite dehydrogenase provide insights into nicotinamide cofactor regeneration. *Biochemistry* **2012**, *51*, 4263–4270. [[CrossRef](#)]
30. Robinson, W.E.; Bassegoda, A.; Reisner, E.; Hirst, J. Oxidation-State-Dependent Binding Properties of the Active Site in a Mo-Containing Formate Dehydrogenase. *J. Am. Chem. Soc.* **2017**, *139*, 9927–9936. [[CrossRef](#)]
31. Gladyshev, V.N.; Boyington, J.C.; Khangulov, S.V.; Grahame, D.A.; Stadtman, T.C.; Sun, P.D. Characterization of crystalline formate dehydrogenase H from *Escherichia coli*. Stabilization, EPR spectroscopy, and preliminary crystallographic analysis. *J. Biol. Chem.* **1996**, *271*, 8095–8100. [[CrossRef](#)]
32. Rivas, M.G.; Gonzalez, P.J.; Brondino, C.D.; Moura, J.J.; Moura, I. EPR characterization of the molybdenum(V) forms of formate dehydrogenase from *Desulfovibrio desulfuricans* ATCC 27774 upon formate reduction. *J. Inorg. Biochem.* **2007**, *101*, 1617–1622. [[CrossRef](#)] [[PubMed](#)]
33. Glasoe, P.K.; Long, F. Use of glass electrodes to measure acidities in deuterium oxide1, 2. *J. Phys. Chem.* **1960**, *64*, 188–190. [[CrossRef](#)]
34. Axley, M.J.; Grahame, D.A.; Stadtman, T.C. *Escherichia coli* formate-hydrogen lyase. Purification and properties of the selenium-dependent formate dehydrogenase component. *J. Biol. Chem.* **1990**, *265*, 18213–18218. [[CrossRef](#)] [[PubMed](#)]
35. Field, L.D.; Lawrenz, E.T.; Shaw, W.J.; Turner, P. Insertion of CO₂, CS₂, and COS into Iron(II)–Hydride Bonds. *Inorg. Chem.* **2000**, *39*, 5632–5638. [[CrossRef](#)] [[PubMed](#)]
36. Diefenbacher, J.; Piwowarczyk, J.; Marzke, R.F. Note: Solution NMR probe for the study of CO₂ sequestration at elevated pressure and temperature. *Rev. Sci. Instrum.* **2011**, *82*, 076107. [[CrossRef](#)] [[PubMed](#)]
37. Gombler, W. NMR-spektroskopische Untersuchungen an Chalkogenverbindungen, III ⁷⁷Se- und ¹⁸C-NMR-Daten von Verbindungen mit C=S- und C=Se-Doppelbindung / NMR Spectroscopic Studies on Chalcogen Compounds, III ⁷⁷Se and ¹³C NMR Data of Compounds Containing C=S and C=Se Double Bonds. *Z. Naturforsch. B* **1981**, *36*, 1561–1565. [[CrossRef](#)]
38. Stueber, D.; Patterson, D.; Mayne, C.L.; Orendt, A.M.; Grant, D.M.; Parry, R.W. Carbonates, Thiocarbonates, and the Corresponding Monoalkyl Derivatives. 1. Their Preparation and Isotopic ¹³C NMR Chemical Shifts. *Inorg. Chem.* **2001**, *40*, 1902–1911. [[CrossRef](#)]
39. Zheng, Y.; Zheng, W.; Zhu, D.; Chang, H. Theoretical modeling of p K_a's of thiol compounds in aqueous solution. *New J. Chem.* **2019**, *43*, 5239–5254. [[CrossRef](#)]
40. Rumble, J. *CRC Handbook of Chemistry and Physics*, 102th ed; Taylor & Francis Group: Oxford, UK, 2021.
41. Holleman, A.F. *Anorganische Chemie*; Walter de Gruyter GmbH & Co KG: Berlin, Germany, 2020.
42. Holm, R.H. The biologically relevant oxygen atom transfer chemistry of molybdenum: From synthetic analogue systems to enzymes. *Coord. Chem. Rev.* **1990**, *100*, 183–221. [[CrossRef](#)]
43. Graham, J.E.; Nicks, D.; Zane, G.M.; Gui, Q.; Hom, K.; Hille, R.; Wall, J.D.; Raman, C. How a formate dehydrogenase responds to oxygen: Unexpected O₂ insensitivity of an enzyme harboring tungstopterin, selenocysteine, and [4Fe–4S] clusters. *ACS Catal.* **2022**, *12*, 10449–10471. [[CrossRef](#)]
44. Nair, S.K.; Christianson, D.W. Crystallographic studies of azide binding to human carbonic anhydrase II. *Eur. J. Biochem.* **1993**, *213*, 507–515. [[CrossRef](#)] [[PubMed](#)]
45. Laun, K.; Duffus, B.R.; Wahlefeld, S.; Katz, S.; Belger, D.; Hildebrandt, P.; Mroginski, M.A.; Leimkühler, S.; Zebger, I. Infrared Spectroscopy Elucidates the Inhibitor Binding Sites in a Metal-Dependent Formate Dehydrogenase. *Chem.–A Eur. J.* **2022**, *28*, e202201091. [[CrossRef](#)] [[PubMed](#)]
46. Laun, K.; Duffus, B.R.; Kumar, H.; Oudsen, J.-P.H.; Karafoulidi-Retsou, C.; Tadjoung Waffo, A.; Hildebrandt, P.; Ly, K.H.; Leimkühler, S.; Katz, S. A minimal light-driven system to study enzymatic CO₂ reduction by a formate dehydrogenase. *ChemCatChem* **2022**, *14*, e202201067. [[CrossRef](#)]
47. Raaijmakers, H.C.; Romao, M.J. Formate-reduced *E. coli* formate dehydrogenase H: The reinterpretation of the crystal structure suggests a new reaction mechanism. *J. Biol. Inorg. Chem.* **2006**, *11*, 849–854. [[CrossRef](#)]
48. George, G.N.; Colangelo, C.M.; Dong, J.; Scott, R.A.; Khangulov, S.V.; Gladyshev, V.N.; Stadtman, T.C. X-ray absorption spectroscopy of the molybdenum site of *Escherichia coli* formate dehydrogenase. *J. Am. Chem. Soc.* **1998**, *120*, 1267–1273. [[CrossRef](#)]
49. Oliveira, A.R.; Mota, C.; Klymanska, K.; Biaso, F.; Romão, M.J.; Guigliarelli, B.; Pereira, I.C. Spectroscopic and Structural Characterization of Reduced *Desulfovibrio vulgaris* Hildenborough W-FdhAB Reveals Stable Metal Coordination during Catalysis. *ACS Chem. Biol.* **2022**, *17*, 1901–1909. [[CrossRef](#)]
50. Meneghello, M.; Uzel, A.; Broc, M.; Manuel, R.R.; Magalon, A.; Pereira, I.A.; Léger, C.; Walburger, A.; Fourmond, V. Electrochemical Kinetics Support a Second Coordination Sphere Mechanism in Metal-Based Formate Dehydrogenase. *Angew. Chem. Int. Ed.* **2022**, *62*, e202212224.
51. Gutteridge, S.; Tanner, S.J.; Bray, R.C. Comparison of the molybdenum centres of native and desulpho xanthine oxidase. The nature of the cyanide-labile sulphur atom and the nature of the proton-accepting group. *Biochem. J.* **1978**, *175*, 887–897. [[CrossRef](#)]

52. Muraoka, M.; Yamamoto, T.; Enomoto, K.; Takeshima, T. Synthesis of 2-alkoxycarbonyl enamino thioaldehydes and selenaldehydes (as pentacarbonyltungsten(0) complexes). Improved synthesis of simple and 2-cyano enamino thioaldehydes and some chemical reactions of these compounds. *J. Chem. Soc. Perkin Trans. 1* **1989**, *7*, 1241–1252. [[CrossRef](#)]
53. Engler, R.; Gattow, G. Über Chalkogenolate. LIII. Untersuchungen über Thioameisensäuren 1. Darstellung und Eigenschaften von Monothioformiaten und Monothioameisensäure. *Z. Anorg. Allg. Chem.* **1972**, *388*, 78–88. [[CrossRef](#)]
54. Lamarre, S.G.; MacMillan, L.; Morrow, G.P.; Randell, E.; Pongnopparat, T.; Brosnan, M.E.; Brosnan, J.T. An isotope-dilution, GC–MS assay for formate and its application to human and animal metabolism. *Amino Acids* **2014**, *46*, 1885–1891. [[CrossRef](#)] [[PubMed](#)]

Disclaimer/Publisher’s Note: The statements, opinions and data contained in all publications are solely those of the individual author(s) and contributor(s) and not of MDPI and/or the editor(s). MDPI and/or the editor(s) disclaim responsibility for any injury to people or property resulting from any ideas, methods, instructions or products referred to in the content.